FISEVIER

Contents lists available at ScienceDirect

Journal of Hydrology: Regional Studies

journal homepage: www.elsevier.com/locate/ejrh



The role of peat-forming bofedales in sustaining baseflow in the humid puna[☆]

Wyeth Wunderlich ^a, Margaret Lang ^b, Kristina Keating ^c, Wilner Bandera Perez ^d, Jasper Oshun ^{c,e,*}

- ^a California Polytechnic University, Humboldt, Department of Geology, USA
- ^b California Polytechnic University, Humboldt, Department of Environmental Resources Engineering, USA
- ^c Rutgers University Newark, Department of Earth and Environmental Sciences, USA
- ^d Universidad Nacional de San Antonio Abad del Cusco (UNSAAC), Departamento de Geología, Peru
- ^e US Fulbright Scholar and Visiting Professor at the Universidad de Ingeniería y Tecnología (UTEC), Lima, Peru

ARTICLE INFO

Keywords: Bofedales Puna Water resources Wetlands Natural infrastructure Nuclear magnetic resonance

ABSTRACT

Study region: Humid puna of the Central Andes, Perú

Study focus: Bofedales, or peat-forming wetlands, are a characteristic feature of the humid puna - a high elevation, seasonally dry grass- and shrub-land throughout the Central Andes. Despite the hydrologic importance of the humid puna for downstream communities, and the inference that bofedales play an important role, few studies have explored the hydrology of this ecosystem, and none have quantified bofedal water yield to streams. We designed a 3-year study in the Upper Ramuschaka Watershed (URW), a 2.12 km² humid puna catchment sustaining a perennial stream used for irrigation downstream. We monitored hydrologic fluxes through the URW, periodically measured discharge in 19 nested subbasins across wet and dry seasons, and characterized the structure, hydraulic properties, and storage capacity of four bofedales.

New hydrological insights for the region: Unit runoff is consistently higher in subbasins with greater bofedal coverage. High porosity peat fills in the wet season via groundwater recharge and drains slowly through underlying layers with low hydraulic conductivity. Bofedales cover 11.6% of the URW and store $105,000\pm10,000~{\rm m}^3$ of water seasonally. In the dry season, bofedales yield $49\pm5~{\rm mm}$ to streams, equivalent to 20-98% of the URW's dry season runoff. Bofedales regulate drainage from the humid puna to downstream communities and are therefore vital to local and regional water security.

1. Introduction

The 'humid' or 'wet' puna is a seasonally dry grass- and shrub-land located above the tree line that sustains perennial streams and provides water to downstream communities throughout the Central Andes (e.g., Buytaert et al., 2009, Josse et al., 2009; Drenkhan et al., 2015; Ochoa-Tocachi et al., 2016). The humid puna is found between 8° S and 15° S latitude, at elevations between 2000 and 6000 m.a.s.l., covering an estimated 18.6% (236,220 km²) of the Tropical Andes from central Perú through northeastern Bolivia (e.g.,

https://doi.org/10.1016/j.ejrh.2023.101394

Received 5 May 2022; Received in revised form 10 April 2023; Accepted 19 April 2023 Available online 16 May 2023

2214-5818/© 2023 The Authors. Published by Elsevier B.V. This is an open access article under the CC BY-NC-ND license (http://creativecommons.org/licenses/by-nc-nd/4.0/).

^{*} To our parents. You will always be with us.

^{*} Corresponding author at: Rutgers University Newark, Department of Earth and Environmental Sciences, USA. *E-mail address*: jo560@scarletmail.rutgers.edu (J. Oshun).

Josse et al., 2009). Under the Intergovernmental Panel on Climate Change (IPCC) carbon emissions scenario A1B (1° C to 1.5° C projected regional temperature increase), an estimated 21.6% of glacierized and cryoturbated land area in the Tropical Andes will be replaced by humid puna from 2010 to 2039 (Tovar et al., 2013). As the climate warms and the humid puna migrates upslope, understanding and predicting changes to local and regional hydrologic processes will be vital to future water security.

Mean annual precipitation in the humid puna varies from 600 mm to 2000 mm, resulting in a wetter climate than the dry puna found in Argentina and Chile and a drier climate than the jalca and páramo biomes of the northern Andes (Squeo et al., 2006; Josse et al., 2009; Tovar et al., 2013; Ochoa-Tocachi et al., 2016). Precipitation falls primarily between December and April, with a near-absence of precipitation from May to August (e.g., Squeo et al., 2006; Garreaud, 2009; Drenkhan et al., 2015; Ochoa-Tocachi et al., 2016; Aybar et al., 2020). Hydrographs of streams throughout the puna track seasonal inputs of precipitation and runoff is driven primarily by groundwater drainage (e.g., Baraer et al., 2009; Somers et al., 2019; Buytaert et al., 2017; Glas et al., 2019; Somers et al., 2019; Fernandez-Palomino et al., 2021).

The complex topography of the puna landscape includes glacial features such as steep, amphitheater-shaped uplands draining to low gradient basins filled with quaternary fluvial, glaciofluvial, and/or colluvial deposits (Josse et al., 2009; Ochoa-Tocachi et al., 2016; Somers and McKenzie, 2020). These basins host wetlands known as 'bofedales' (singular: 'bofedal') - seasonally or perennially saturated peat-forming wetlands with distinct hydrophytic plant assemblages found in topographic depressions, valley bottoms, and along watercourses within the humid and dry puna (e.g., Cooper et al., 2019; Squeo et al., 2006; Maldanado Fónken, 2014; Polk et al., 2019). Bofedal extent in the Peruvian Andes is estimated to be nearly 550 km² (Ministry of the Environment, 2019).

Recently, bofedales have been referred to as 'natural' or 'green' infrastructures (e.g., Argüello, 2018; Castillo and Crisman, 2019; López Gonzales et al., 2020) that seasonally capture, store, and release water; therein regulating water yield from hillslopes to streams (e.g., Earle et al., 2003; Flores et al., 2014; Maldanado Fónken, 2014). Here, we use the words 'natural' and 'green' while acknowledging many bofedales are 'socio-hydrological' systems (e.g., Yager et al., 2021), or 'cultural landscapes' (e.g., White-Nockleby et al., 2021). Indeed, bofedales have long provided grazing grounds for Andean camelids (e.g., Palacios Rios, 1977; Bryant and Farfan, 1984; Reiner and Bryant, 1986; Patty et al., 2010), and have been managed and expanded to sustain local water resources (Flores-Ochoa, 1977; Palacios Rios, 1977; Erickson, 2000; Lane, 2009; Vining et al., 2019; Uribe-Álvarez et al., 2022). Bofedales have also been linked to the presence and expansion of human settlements (e.g., Vining et al., 2019).

Two properties of bofedales contribute to their inferred role as a natural water storage infrastructure. First, bofedales contain layers of high porosity peat up to 10 m thick (Hribljan et al., 2015; Engel et al., 2014; Cooper et al., 2019) with the capacity to store large quantities of water (e.g., Cooper, 2019; Valois et al., 2020; Valois et al., 2021). Secondly, as post-glacial features, bofedales are often found in low gradient areas fed by large contributions of upslope groundwater (e.g., Gordon et al., 2015; Cooper et al., 2019). Although they are peat-forming, bofedales are minerotrophic fens, meaning water and nutrients primarily come from groundwater. Fens differ from ombrotrophic bogs, which receive water and nutrients from precipitation only (Squeo, 2006; Cooper et al., 2010, 2019; Maldonado Fónken, 2014; Salvador et al., 2014; Hribljan et al., 2015; Oyague et al., 2022).

The hydrologic role of peat-forming wetlands has been studied to the north and south of Perú. In the humid páramo of Ecuador, annual water yield and catchment-wide water storage increase with the extent of peat-forming wetlands (Mosquera et al., 2015; Lazo et al., 2019). In the arid Andes of North-Central Chile, geophysical and hydrochemical methods revealed bofedales to have large total water storage due to their large average porosity (Valois et al., 2020; Valois et al., 2021). Whereas these studies identify links between wetlands, water storage, and flow regulation, no study has yet quantified the annual amount of water bofedales seasonally store and release to streams.

Our study focused on the Upper Ramuschaka Watershed (URW), a headwater catchment within the 11,048 km² Vilcanota–Urubamba Basin (VUB) (Drenkhan et al., 2018). The humid puna covers 78.2% of the VUB (Oshun et al., 2021; Josse et al., 2009), and the hydrograph is driven by groundwater draining the humid puna (Drenkhan et al., 2015; Buytaert et al., 2017; EGEMSA, Oshun et al., 2021; Fernandez-Palomino et al., 2021). Cusco, the largest city in the VUB with a population of approximately 420,000 (INEI, 2015), derives approximately 90% of its water from the humid puna (SEDACUSCO, 2019). The URW, which is a non-glacierized watershed characteristic of the humid puna, is the primary local water source for the agrarian district of Zurite (population of 3640; Municipalidad Distrital de Zurite, 2017). Zurite is vulnerable to water shortages due to a dependence on limited local water resources, a pronounced dry season, and a lack of long-term water storage. The dry season (May – October) water demand for the 852-irrigated hectares in Zurite is ~ 1150 mm (Municipalidad Distrital de Zurite, 2017).

The URW represents an example watershed in the humid puna that may provide insights into to hydrologic processes across the region. Specifically, we addressed the following questions:

- 1) What are the annual and seasonal water yields from the URW, a humid puna catchment in the Central Andes?
- 2) What are the temporal patterns linking subsurface hydrology and streamflow in the URW?
- 3) Is there a relationship between bofedal area and unit runoff (hereafter referred to as runoff) in the URW?
- 4) What is the quantity of seasonally dynamic water storage in bofedales and what proportion of total dry season runoff is released from bofedales? Here, we define seasonally dynamic storage relative as the volume of water stored in bofedales relative to the end of the dry season (e.g., Sayama et al., 2011).

We collected hydrogeologic data over three water years through the collaborative effort of students, scientists, and community members (Oshun et al., 2021). Our results provide hydrologic data from a societally important, yet understudied region, and show water released in bofedales is partly responsible for sustained dry season streamflow.

2. Materials and methods

2.1. Site description of the Upper Ramuschaka Watershed (URW)

The 2.12 km^2 URW spans elevations of 4011 - 4543 m.a.s.l. and sustains three perennial streams draining three primary subbasins – the Western, (0.373 km^2) , Central (0.873 km^2) , and Eastern (0.797 km^2) (Fig. 1). These subbasins form a confluence $\sim 150 \text{ m}$ upstream of the terminus of the URW, at a concrete diversion weir used by the community of Zurite to divert surface water for irrigation. Mean annual precipitation (1981 - 2017) in Zurite (3405 m.a.s.l.) is 848 mm, 95% of which falls between October and April (Aybar et al., 2020).

The underlying bedrock of the URW is primarily the Eocene-age San Jeronimo Formation (Fig. S1). The Central and Eastern subbasins are underlain by cliff-forming reddish-gray sandstone that is finely-bedded to massive, locally known as 'Capa Roja' (e.g., Carlotto et al., 2010; García Fernández Baca, 2017). The sandstone is interbedded with broad sections of tan to reddish gray to greenish gray finely-bedded and extensively fractured weak mudstone, known as *lutita* (e.g., García Fernández Baca, 2017). A sugary-white crystalline quartzite forms a steep bedrock-exposed ridge that divides two upper tributaries of the Central subbasin. The Western subbasin is underlain by the San Jeronimo Formation; however, there is also extensively weathered limestone karst in the northwest, and an Oligocene quartz monzodiorite intrusive underlying the southwest portions of the subbasin, respectively.

The topography and vegetation are characteristic of the humid puna. The URW headwaters are defined by cliff forming headwalls of quartzite or sandstone and more gently sloping *lutita*. Below are low gradient valleys with seasonally saturated bofedales, poorly distinguished moraines at the margins, and hummocky landforms (Fig. 2). The topography of the landscape combined with its southern aspect suggest recent glaciation, perhaps during the Holocene.

Steep uplands are predominantly covered in the perennial tussock grass, *Jarava ichu*, which we observed to be rooted to a depth of approximately 1.2 m. Hydrophytic plants, such as *Distichia muscoides*, *Oxychloe andina*, and *Plantago tabulosa* are found in the seasonally saturated bofedales. There is no *Sphagnum* moss, which is consistent with the *Distichia* peatlands presented in Maldanado Fónken (2014). To stabilize hillslopes following landslides, the community of Zurite planted *Polylepis sp.* in a grid pattern over an area

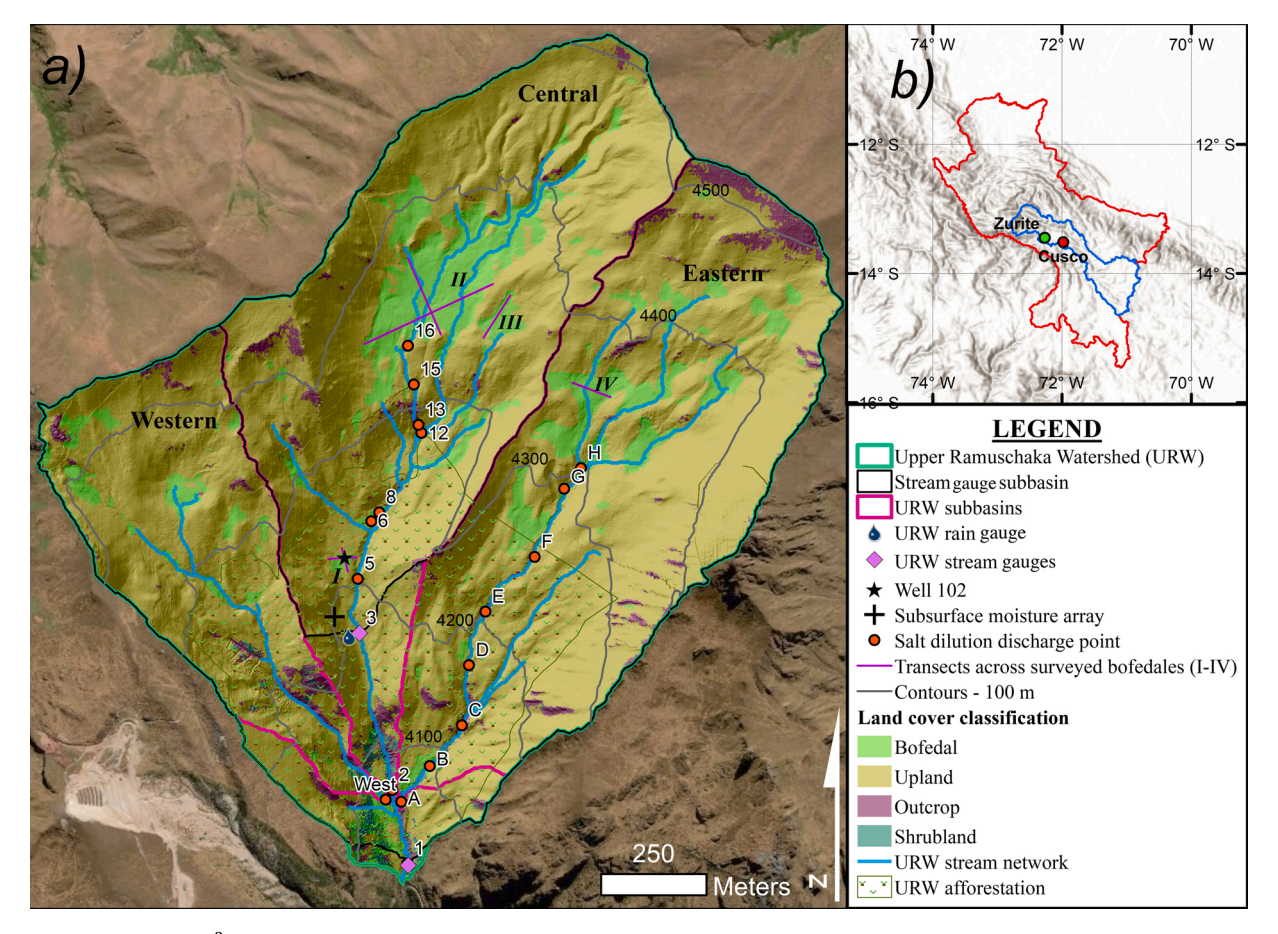


Fig. 1. a) The 2.12 km² Upper Ramuschaka Watershed, which is b) located in the Vilcanota Urubamba Basin (blue outline) in the department of Cusco (red outline). The URW has four primary land cover types: Bofedal, Upland, Outcrop, and Shrubland. Each of the three basins – the Western, Central and Eastern – yield perennial streamflow. Italic Roman numerals show the locations of sampled bofedales. Numbers and letters show the locations of distributed discharge measurements in the Central and Eastern subbasins, respectively. Native tree (Polylepis sp) afforestation occurred in the lower part of the watershed in January 2018.

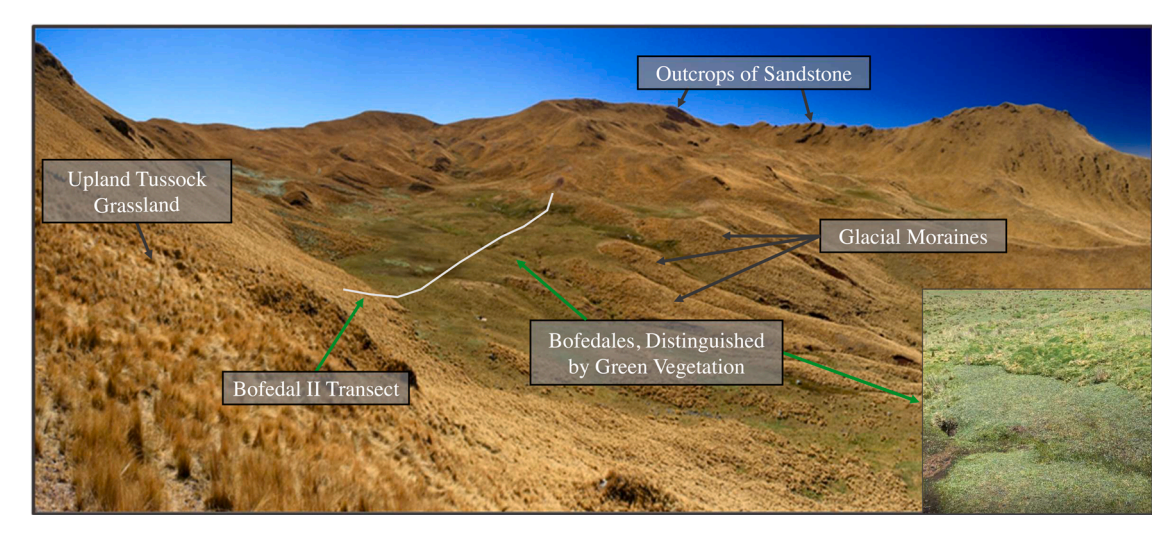


Fig. 2. The view (looking to the northeast) over bofedal II, the largest in the Upper Ramuschaka Watershed at 0.085 km². The white line shows the downhole nuclear magnetic resonance transect. The ridgeline above the bofedal is the upper boundary of the Central Basin. The ridgeline from the center of the photograph to the right defines the boundary of the Eastern Basin. The photograph shows three of the four defined landcovers: Bofedal, Upland covered in *J. ichu,* and Outcrop. Shrubland is found only in the lower reaches of the catchment.

of 0.568 km² in the lower URW (Fig. 1). Despite the afforestation campaign, most *Polylepis* shrubs remained small (< 1 m in height, with sparse branching) because of low growth rates through seasonal drought and a grassland fire in late July 2019.

Soils beneath *J. ichu* are dark and organic rich (20-25%) silt loams to approximately 0.25 m, underlain by dark silty clay loam to sandy loam with organic content decreasing to 7% or less. Sand and rock chips increase in concentration with depth with transition to a fractured and weathered saprolite at depths of 0.4-0.75 m. In comparison to the Andosols of the humid páramo (e.g., Buytaert et al., 2005; Mosquera et al., 2020a, b), upland soils in the URW are derived from primarily sedimentary parent material, exhibit a thinner organic-rich layer, generally less clay-sized particles (<40% in the soil and 5-29% in the saprolite), a well-developed B horizon, and the absence of a low conductivity layer and seasonally perched water table.

2.2. Geospatial characterization

2.2.1. Land cover classification

We used the support vector machine algorithm (L3Harris Geospatial, 2019) on a 1-meter resolution image of the URW (ESRI World Imagery) to classify four land cover classes in the URW: 'Bofedal', 'Upland', 'Outcrop' and 'Shrubland'. We quality controlled the resulting land cover classification vectors via ground truthing during field campaigns and with orthoimagery (8.3 cm/pixel) produced from Unmanned Aerial Vehicle (UAV) surveys.

2.2.2. Topographic data collection and processing

In June 2019, we flew a DJI Phantom 4 Pro UAV to create a Digital Elevation Model (DEM) of the URW. We programmed flights to take photos with 80% coverage overlap at 200 feet above the ground surface and used a Real Time Kinematic (RTK) GPS (EOS, ArrowGold) to survey 26 Ground Control Points (mean horizontal error of 0.097 m and mean vertical error of 0.113 m; Supplementary Material, S2). We post-processed imagery in Agisoft Metashape Professional to create a 1-m/cell resolution DEM following protocols from the United States Geological Survey (2017) and Dietrich (2015). The mean slope of the URW (for 1 m pixels) is 24.0° (Table 1), however the mean slope of bofedales, which cover 0.244 km² (11.6% of the URW), is 14.1°.

Table 1
The total area and mean slope for 1 m pixels of each land cover type in the URW.

Land Cover Type	Area (km²)	Mean Slope (degrees)	
Ichu Upland	1.766	24.2	
Bofedal	0.244	14.1	
Outcrop	0.089	35.4	
Shrubland	0.014	37.0	
URW (all land covers)	2.12	24.0	

2.3. Hydrologic monitoring

2.3.1. Annual water balance

We constructed annual water balances by measuring precipitation (P) and runoff (q), calculating actual evapotranspiration (ET_a), and estimating interannual water storage (ΔS). Water balances are referenced to the Site 3 gauging station in the Central subbasin (0.806 km², Fig. 1). Due to the incomplete data set for Water Year (WY) 2019, which lacked a complete record of upland soil and saprolite and groundwater measurements used to estimate ET_a , we focused our water balance analyses on WY2020 and WY2021.

2.3.2. Precipitation

Precipitation was measured at a resolution of 0.2 mm using a tipping bucket rain gauge (HOBO Onset RG3) installed in June 2018 near Site 3 at a height of approximately 1.5 m above the ground. The start of the annual water year (September 1) corresponds with the end of the regionally dry austral winter and marks a gradual transition into the wet season. We define the dry season as the period over which 15-day cumulative precipitation remained less than 10 mm and the wet season as the period over which 15-day cumulative precipitation exceeded 10 mm.

Although spatial variability in precipitation can be high in Andean catchments (e.g., Buytaert et al., 2006a; Célleri et al., 2007), the rugged topography and limited access prevented us from installing a spatially distributed rainfall network. The rain gauge was installed near the geographic center of the URW, at 4171 m.a.s.l.

The resolution of the national gridded precipitation dataset (Aybar et al., 2020) is insufficient to show variability within the URW. For our water balance estimates, we corrected for orographic effects via an elevation-precipitation model using rain gauges in the URW and Zurite (3411 m.a.s.l.). We calculated the difference in 15-day cumulative precipitation between the two gauges and extrapolated (via a second-degree polynomial) to predict annual precipitation at the mean elevation of the Site 3 subbasin (4369 m.a.s.l.) (S3.1).

2.3.3. Bofedal groundwater

In June 2019, we drilled to 11 m in bofedal I (Fig. 1) using a 2.75'' diameter gas powered rotary drill and installed monitoring Well 102. The upper 0.6 m were peat, which was underlain by clay to a depth of 2.5 m. We encountered a layer of weathered bedrock clasts, silt, and clay material interpreted to be glacio-fluvial deposits at 2.5 m, which extended down through the base of the well. We cased Well 102 with 65 mm diameter PVC pipe (with ~ 1 mm slits over the entire length) capped at the base, and installed a pressure transducer (HOBO U20–001) at a depth of 6.93 m to measure water table dynamics. Fully slotted wells have been effective in similar landscapes to monitor bofedal groundwater dynamics (Hribljan et al., 2015; Cooper et al., 2019; Oyague et al., 2022; Monge-Salazar et al., 2022; and Lahuatte et al., 2022).

2.3.4. Streamflow

In June 2018, we installed stream gauges in the Central subbasin (Site 3, drainage area: 0.806 km²) and above the diversion canal (Site 1, drainage area: 2.11 km²). At each location, we connected a slotted PVC staff gauge (with demarcations to 1/50th of a foot) to rebar stakes driven into the channel bed and installed a pressure transducer (HOBO U20L-001) inside the PVC. An identical transducer was installed adjacent to the stream to measure atmospheric pressure. Data were post-processed to account for sensor drift or slight changes in the position of the sensor after downloading data and reinstalling the gauge (S3.2).

Due to high flow variability, narrow (<1 m), shallow (<0.5 m), and steep (>5%) channels with complex streambed morphology, we measured stream discharge using the dry injection salt dilution technique (Hudson and Fraser, 2005), which is more accurate than the area-velocity method in Andean streams (Parra et al., 2016). For each discharge measurement we placed a conductivity probe (Onset U24–001) in the stream and injected a known mass of salt at least 20 channel widths upstream (typically ~15 m upstream). Measurements took 15-20 min. We applied the Conductivity Assistant non-linear correction in Hoboware Pro (Onset) to convert breakthrough curves to specific conductance, and then scaled by the recommended correction factor of 0.486 (Hudson and Fraser, 2005). Additional details can be found in S3.2. At Site 3, we developed two rating curves: one before and one after a high flow event in March 2019. At Site 1, we present one rating curve – from April 2019 onward – due to substantial changes in the channel geometry in March 2019. All three rating curves are well constrained ($R^2 > 0.95$) (Figs. S5, S6). We scaled discharge by watershed area (using the UAV derived 1-m resolution DEM) and present hydrographs of runoff (mm/day) for WYs 2019–2021. Runoff at Site 3 was used in water balances for WYs 2020 and 2021 as it has the longest continuous record and the most well-constrained rating curve. Error in runoff was quantified as the mean residual error from all discharge measurements used to develop each rating curve.

2.3.5. Subsurface moisture monitoring and estimates of grassland evapotranspiration

In January 2019, we installed four Teros-12 volumetric water content (VWC) sensors and two Teros-21 water potential sensors (Meter Group Inc., 2018) at an elevation of 4195 m.a.s.l. beneath a 36° slope covered in *J. ichu* (Fig. 1). An organic rich loam extended to a depth of 0.4 m. Below was a dark brown clayey soil with clasts of sandstone that increased with depth. A transition to sandstone saprolite occurred at 0.75 m and clay content decreased with increasing depth. Roots were found throughout the profile but in decreasing abundance with depth. Bulk density increased from 0.60 g/cm³ at 0.11 m to 0.93 g/cm³ at 0.52 m. The profile was representative of upland soils (Table S4). Probes were inserted horizontally in the upslope face undisturbed soil and saprolite. We installed VWC sensors at depths of 0.2, 0.6, 0.9, and 1.2 m and collocated water potential sensors at depths of 0.2 and 0.9 m. We converted 15-minute VWC measurements to daily averages and multiplied over thicknesses determined by material properties to quantify dynamics in moisture storage (mm) in the soil (0 – 0.75 m) and in the saprolite (0.75 – 1.35 cm) (Table S5).

To estimate ETa from J. ichu, we applied a conditional model depending on whether subsurface conditions were above or below

field capacity. We used in situ measurements of water potential and VWC at 0.2~m (soil) and 0.9~m (saprolite) to construct wetting and drying water release curves (WRC) (Fig. S8). We estimated field capacity using a water potential of -33~kPa. The VWC of field capacity at 0.6~and 1.2~m (where no water potential sensors were installed) was estimated using water potential data at 0.2~m (soil) and at 0.9~m (saprolite), respectively. The VWC's at field capacity in the soil ($0.432, 0.357~cm^3/cm^3$, Table S6) are smaller than those reported in the organic-rich Andosols of the humid páramo (e.g., Buytaert et al., 2005; Mosquera et al., 2020), which may be due to the lower organic matter content at our study site.

When subsurface moisture at 0.2 m depth exceeded field capacity (0.432), we calculated a daily reference evapotranspiration (ET $_0$) via a temperature-based model (Visualizing Ecosystem Land Management Assessment 2.0, Abdelnour et al., 2011; Hamon, 1963). We then converted ET $_0$ to actual evapotranspiration, ET $_a$, by scaling by a crop coefficient of 0.74, which was recently derived for the 'less humid period' in humid páramo grasslands (Carrillo-Rojas et al., 2019). When water potential in the soil fell below field capacity, we integrated moisture losses (in mm) over the rooting zone using the VWC sensors. There were 202 and 159 days in which field capacity was exceeded in WY 2020 and 2021, respectively. We extrapolated the ET $_a$ estimates to land classified as Upland, which covers 83% of subbasin 3. Error estimates of the Teros-12 sensors is reported to be + /- 3.00% for an uncalibrated mineral soil system such as the URW upland (Meter Group, Inc, 2019). However, to account for error in our field capacity estimates, the temperature-based method for deriving ET $_0$, and our crop coefficient, we applied the maximum error (+/- 30%) reported from estimates in the humid páramo (Córdova et al., 2015).

2.3.6. Estimates of bofedal evapotranspiration

To estimate daily ET_a fluxes from bofedales (covering 16% of the Site 3 subbasin), we calculated daily ET_a using VELMA (as above) and converted ET_a by applying a crop coefficient of 0.85 derived from a study of peat bogs (Gerling et al., 2019). We applied the same maximum error from above (+/- 30%) to our estimates of bofedal ET_a .

2.4. Spatiotemporal measurements of discharge

We measured discharge via salt dilution (Hudson and Fraser, 2005) at 19 nested locations on 14 dates between June 2019 and September 2021 within the Central (n=10), Eastern (n=8), and Western (n=1) subbasins (Fig. 1). The monitoring strategy was designed to measure the spatial and temporal variability of runoff and to compare runoff to the extent of bofedales across the URW's subbasins. We hypothesized that subbasins with greater percent bofedal cover would yield higher runoff, especially in the dry season. Our measurements focused on the Central and Eastern subbasins because the underlying lithologies are consistent (Fig. S1). The drainage areas of the subbasins range from 0.096 to $2.112 \, \mathrm{km}^2$, with bofedales covering 7.71-29.42% (Table S1). Channel morphology ranged from relatively gentle-sloped reaches flowing through bofedal and wet grassland settings to steep bedrock-confined channels predominantly found in the lower portion of the watershed. In most locations, the channel was incised into either bedrock, proglacial features, or bofedales.

2.5. Seasonal moisture dynamics in bofedales

2.5.1. Material and hydraulic properties of bofedales

To characterize material and hydraulic properties in bofedales, we augered 34 boreholes in transects spanning ichu uplands immediately above and through bofedales 'I' (2 transects, 9 boreholes), 'II' (2 transects, 15 boreholes), 'III' (1 transect, 5 boreholes), and 'IV' (1 transect, 5 boreholes) (Fig. S7). Ten boreholes were used for nuclear magnetic resonance (NMR) surveys and were augered with a 2.25'' bucket; all other boreholes were augered with a 4'' bucket. Boreholes were augered in June 2019 (dry season) and January 2020 (wet season). Peat was field identified by a very dark brown to black color, partially to completely decomposed organic matter, a greasy and fibrous texture, and high-water content when saturated (yielded water when squeezed). We corroborated field estimates with laboratory data showing gravimetric water contents (from 0.6 to $1.45 \, \mathrm{g} \, \mathrm{g}^{-1}$), weight percent carbon (25 - 45%), and total porosities exceeding 0.8. Clay was identified by an increase in density, dark gray to reddish gray color, the disappearance of organic matter, and the ability to roll soil into 'worms'. Silt, sand, and rock chips increased with depth due to glacio-lacustrine and fluvial deposits or weathered bedrock, henceforth referred to as the 'mineral layer.'

In June 2019, we surveyed 10 boreholes in bofedales I and II with a portable downhole NMR Logging System (Dart, Vista Clara, Inc., Mukilteo, Washington, USA). NMR is a geophysical method that directly detects the presence of hydrogen and is used to determine porosity or water content, and to estimate hydraulic conductivity (e.g., Behroozmand et al., 2015). Unlike other in situ methods for determining water content, such as neutron probe and time domain reflectometry, NMR estimates of water content do not require site specific calibration (e.g., Schmidt and Rempe, 2020). Measurements were made with 0.25 m spacing from the ground surface downward. Each measurement's investigation volume was a cylindrical shell of 0.23 m height, 1–2 mm in thickness at a radius of 6.5–7.6 cm from the central axis of the tool (Walsh et al., 2013). Additional details on instrument parameters and data processing can be found in S4.1.

2.5.2. Estimates of bofedal dynamic water storage

We quantified seasonally dynamic water storage in bofedales (storage relative to the end of the dry season), through downhole NMR measurements, direct observations of material properties and saturation state, and water table monitoring in bofedal I.

For each layer (peat, clay, mineral) we calculated drainable water storage as the difference between NMR measurements of total porosity (VWC at saturation) and an estimation of VWC at field capacity. We did not measure water potential in the peat so we could not construct WRCs as we did for the upland soils. Instead, we estimated field capacity by measuring the VWC of freely drained peat,

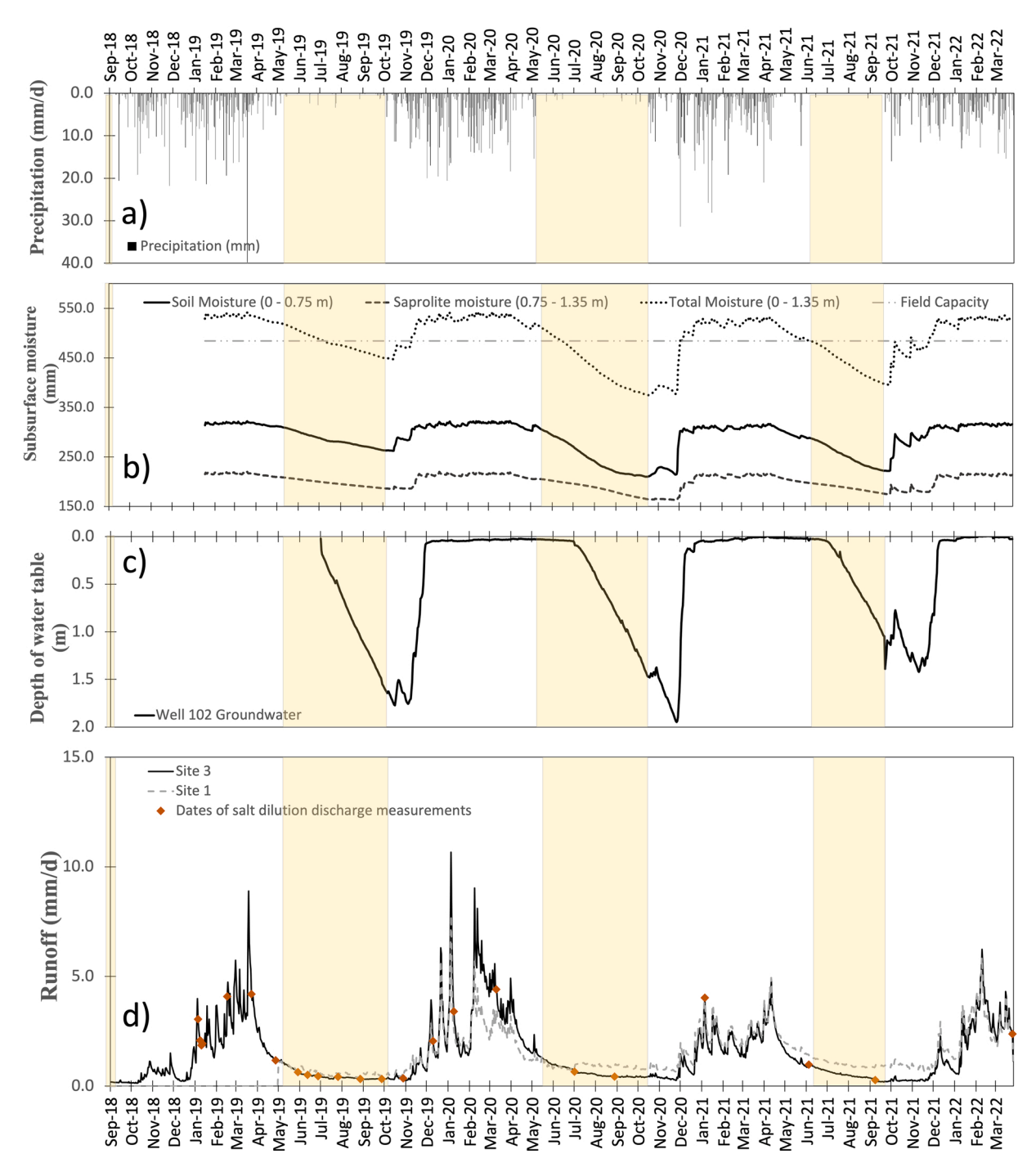


Fig. 3. Time series of hydrological data over the monitoring period (September 2018 – March 2022) showing: a) precipitation in mm/d at the Upper Ramuschaka Watershed rain gauge; b) subsurface moisture storage in soil and saprolite with dashed lines showing estimates of field capacity in the soil and the saprolite; c) groundwater dynamics at Well 102 in the center of bofedal I; and d) runoff in mm/day at Sites 1 and 3. The yellow bands show the dry seasons, when 15-day cumulative precipitation remained below 10 mm. Greater subsurface moisture drying in 2020 (b) is likely due to vigorous vegetation growth following a low-intensity grassland fire in late July 2019.

Table 2Hydrologic metrics for three dry seasons: 2019, 2020, 2021. The dry season is defined as the period when 15-day cumulative precipitation remained under 10 mm.

Dry Season	Number of days	Cum. precip. (mm)	Cum. runoff at Site 3 (mm)	Min. Soil Moisture Storage (mm)	Min. Saprolite Moisture Storage (mm)	Days from onset of dry season until bofedal I desaturated		Max. Water Table Depth in W102 (m)	Min. flow at Site 3 (mm/d)
1: May 8th - Oct 4th, 2019	150	20.6	69.6	262	186	55	15.2	1.77	0.13
2: May 19th - Oct 18th, 2020	153	24.7	93	210	163	43	13.4	1.94	0.25
3: Jun 8th - Oct 1st, 2021	115	10.6	57	222	174	25	13.3	1.42	0.26
Mean	139	19	73	231	174	41	14.0	1.71	0.21

clay, or the mineral layer a distance of approximately 0.25 m above the water table in (peat) or at the margins (clay, mineral layer) of bofedal II. Our estimates for field capacity in peat is $0.42 \text{ cm}^3/\text{cm}^3$, which matches reported values of field capacity in hemic peat (Dimitrov and Lafleur, 2021). Our estimate of field capacity in the clay $(0.3 \text{ cm}^3/\text{cm}^3)$ and mineral layer $(0.2 \text{ cm}^3/\text{cm}^3)$ are supported by previous studies of lacustrine clays (Bruand and Tessier, 2000; Ito and Azam, 2009).

We determined the minimum depth of the water table via direct measurements. Maximum water depth was estimated by continuous monitoring in Well 102 and corroborated with field measurements. In the wet season (January 2020) the average depth to the water table in the four bofedales was 0.12 m (Table S7), with standing water across large portions of all four bofedales. In the dry season (July 2019) the depth to water table was similar across bofedales I and II. The maximum observed water table depth at W102 (1.94 m) was applied to bofedales II – IV. We interpolated layers (peat, clay, mineral) and the maximum and minimum depth of water table across the cross-sections using Inverse Distance Weighting (Figs. S11- 14). We then multiplied the areas of each layer by its drainable VWC to calculate dynamic storage and determine the total for each cross-section. Finally, we divided total storage in each cross-section by the length of the cross-section to estimate average dynamic storage capacity (in mm) for bofedales I – IV.

3. Results

3.1. Annual water balances and dry season runoff

Precipitation, subsurface moisture, groundwater, and runoff dynamics in the URW followed seasonal cycles of wet-up from October to December, a sustained period of precipitation and high runoff from December to April, and a dry period from May to October (Fig. 3).

3.1.1. Precipitation

The precipitation measured in the URW rain gauge was 749, 825, and 738 mm in WYs 2019, 2020, and 2021, respectively. The dry season started in May to early June with an average length of 139 days and average precipitation of only 19 mm (Fig. 3a, Table 2). The onset of the wet season occurred in early- to mid-October and wet season precipitation peaked in frequency and intensity between December and April (Fig. 3a).

3.1.2. Subsurface moisture dynamics in the uplands

In WYs 2020–2022, an average of 138 mm of cumulative precipitation fell before field capacity was reached across the upland rooting depth (Table 3). Successive storms caused ephemeral increases in soil and saprolite moisture storage and drainage to deeper layers. In the dry season, subsurface moisture storage (across the soil) fell below field capacity (Fig. 3b) with faster rates of drying and greater overall moisture loss in the soil. By the end of the dry season, soil and saprolite water storage reached average minimum values of 231 and 174 mm, respectively (Table 2).

Table 3

Hydrologic metrics for the wet-up and wet season of four water years (2019 – 2022). The water year begins on September 1. *In WY 2022, cumulative precipitation was measured at the Casa Zurite rain gauge (3411 m.a.s.l.). Field capacity was estimated as 298 mm in the soil and 178 mm in the saprolite.

WY	Cumulative precipitation before field capacity (mm)	Cumulative precipitation before bofedal I saturated (mm)	Date of bofedal saturation	Cumulative precipitation before runoff exceeded 1 mm/d at Site 3 (mm)		ows at Site 3 and l/s)
2019				145	8.9	83
2020	115	174	11/29/19	177	10.7	100
2021	160	224	12/22/20	206	5	47
2022	140	192	12/11/21	162	6.2	58
Mean	138	197	Dec 11th	173	7.7	72

Table 4Annual water balances referenced to the Site 3 subbasin for WY2020 and WY 2021. Precipitation, runoff, and ET_a (from January 2019 onward) are reported for WY 2019, but no change in storage is calculated due to the incomplete ET_a record. Meter Group sensors were installed in January of 2019. Precipitation values are adjusted to reflect the mean elevation of subbasin 3.

*****		Precipitation			Runoff	n di a lam	
WY Metric		Wet season	Dry season	Wet season Dry season (through WY		Estimated ET _a	ΔS
Total (mm)		776	13	393	59	119 + 36 *	N/A
WY2019	Total (IIIII)	789	\pm 8	452 ± 54		119 ± 30 "	IV/A
	Percent	100%		$57\% \pm 12\%$			N/A
m . 1 ()	Total (mm)	859	8	560	84	293 ± 88	-69
WY2020 Total (mm)		867 ± 4		643 ± 84		293 ± 88	-09
Percent		100	0%		$74\% \pm 13\%$	$34\% \pm 10\%$	8%
WY2021 Total (n	m-+-1 ()	752	2	390	49	064 + 00	
	iotai (mm)	754	754 ± 1		439 ± 57	264 ± 80	51
	Percent	100	0%		$58\% \pm 13\%$	$35\% \pm 11\%$	7%

3.1.3. Bofedal groundwater dynamics

Groundwater dynamics in bofedal I showed remarkably consistent annual cycles of recharge, sustained saturation through the wet season and into the dry season, and steady decline until the following wet up (Fig. 3c). The water table in bofedal I responded immediately to the start of the wet season with a modest rise. However, there was a dramatic rise in the water table to saturation that closely coincided with the timing of field capacity on the hillslopes. Bofedal I saturated between late November and mid-December following an average of 197 mm of cumulative precipitation (Table 3). Bofedal I desaturated an average of 41 days into the following dry season and declined linearly at an average rate of 14.0 mm/day to an average maximum depth of 1.71 m (Table 2).

3.1.4. Runoff in the URW

At the onset of the wet season, runoff rose above values of 1 mm/d after an average of 173 mm of cumulative precipitation, similar to the amount of cumulative precipitation when bofedal I saturated, and exceeding the amount that resulted in field capacity across the *ichu* rooting zone in the hillslope (Fig. 3d, Table 3). Throughout the wet season, runoff at Site 3 responded quickly to precipitation inputs, with peak flows rising to an average of 7.7 mm/d (72 l/s) (Table 3). In WY 2021, low stream stage resulted in peak flows that never exceeded 5.0 mm/d (47 l/s). The site 3 rating curve combined WYs 20 and 21 due to infrequent field visits through the COVID-19 lockdowns. Despite these limitations, medium and low flows were consistent with our rating curve (Figs. S5). Runoff declined steadily as the system entered the dry season. Across the three dry seasons, the rate and shape of runoff recessions were similar with average minimum flow of 0.21 mm/d (2.0 l/s).

3.1.5. Annual water balances

Annual precipitation, adjusted for orographic effects by using the mean elevation of the Site 3 subbasin ranged from 754 to 867 mm over WY 2019 – 2021 (Table 4). Annual precipitation values are within one standard deviation of the long-term (1981–2017) average annual gridded precipitation (848 \pm 156 mm) (Aybar et al., 2020).

Annual runoff varied from 439 to 643 mm, corresponding to 57 - 74% of annual precipitation, with ET_a accounting for 34 - 35%. Dry season runoff amounted to 12% of annual runoff on average.

The difference between annual inputs and outputs (ΔS in Table 4) combines interannual watershed storage, potential drainage below the stream gauge at Site 3 (which we did not directly measure), and measurement error. In WY2020, ΔS was - 69 mm, and in WY2021, ΔS was 51 mm (Table 4).

3.1.6. Temporal phases of the annual water balance

Fig. 4 shows the cumulative fluxes of precipitation, ET_a , and runoff in subbasin 3 for WYs 2020 and 2021. The seasonality of precipitation and the watershed's response (runoff, Et_a , storage in bofedales) are used to separate the water year into three phases: 'fill-up', 'steady-state', and 'release' (values are in Table S8).

The fill-up phase began with the start of the WY (here we use 'fill-up' rather than the more general wet-up used above to specify the period from September 1 until bofedal I saturated). During the fill-up phase, cumulative runoff and ET_a were modest. Cumulative precipitation, which exceeded the combined fluxes of runoff and ET_a by greater than a factor of four, primarily recharged the unsaturated zone.

The steady-state phase began with saturation of bofedal I, which closely followed the rise in moisture to field capacity in the hillslope. In this phase, successive precipitation events caused rapid stormflow responses and cumulative ET_a increased steadily due to increasing temperatures during the austral summer. Precipitation inputs roughly equaled the combined outputs of runoff and ET_a.

The release phase began with the onset of the dry season (May 19 in WY2020, and June 8 in WY2021). Although there is a near absence of precipitation during this phase, cumulative runoff continues to increase as streams continue to flow. Bofedal I did not desaturate until an average of 41 days into the dry season (Table 2). Baseflow throughout the release phase remained above 0.25 mm/d. ET_a accounted for the greatest total moisture loss over the release phase as upland grasses and hydrophytic vegetation sustained steady rates of transpiration, leading to moisture depletion across the root zone.

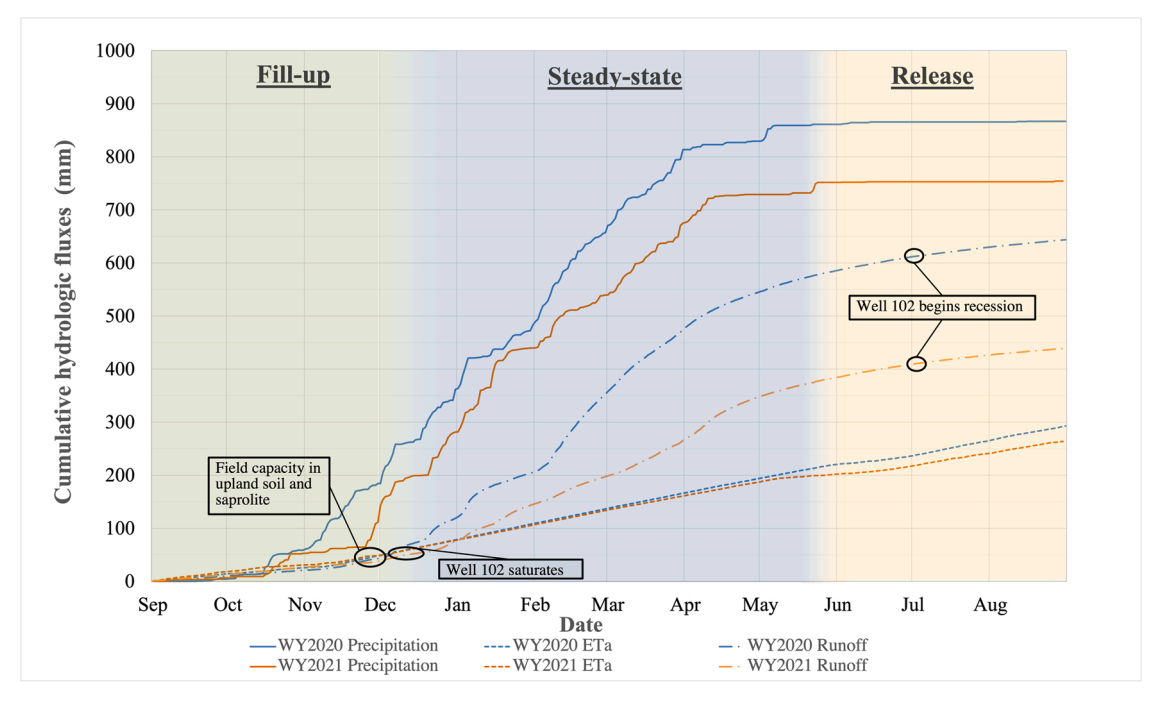


Fig. 4. Cumulative fluxes of water through the Upper Ramuschaka Watershed for water years 2020 and 2021. The seasonality of precipitation and resulting patterns in runoff and evapotranspiration (ET_a) define three phases: fill-up, steady state, and release. The fill-up phase is defined by recharge of the unsaturated zone and groundwater reservoir in bofedal I. In the steady state phase, precipitation is approximately equal to the combined fluxes of runoff and ET_a , and runoff shows large increases. In the release phase, little to no precipitation falls, and cumulative runoff increases slowly due to bofedal drainage. Cumulative precipitation curve corresponds to precipitation adjusted to the mean elevation of subbasin 3.

3.1.7. Spatiotemporal patterns of runoff in the URW

We measured greater runoff across all seasons coming from subbasins with higher bofedal coverage (Fig. 5). Data points are colored corresponding to the flow exceedance probability (across the monitoring period) at Site 3, to indicate the general flow conditions in the URW. The start of the dry season corresponded with the 41.5, 39.3, and 44.5% exceedance flow in WYs 2019–2021, respectively. We performed a simple regression analysis on the percent of the subbasin covered in bofedales and the logarithm of runoff. At high flows

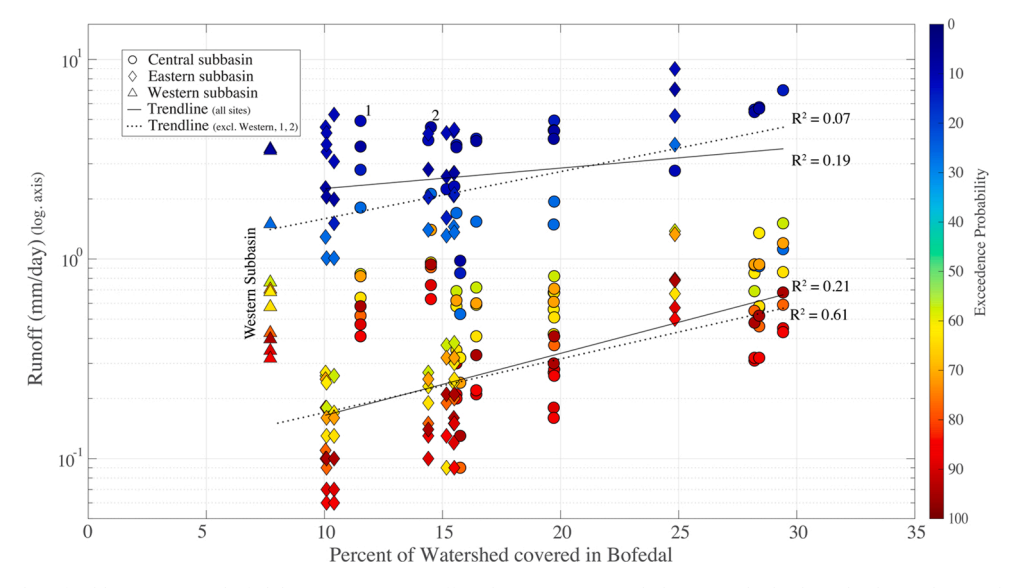


Fig. 5. Scatterplot of subbasin percent bofedal cover versus runoff in the Upper Ramuschaka Watershed. The color-bar indicates the flow percent exceedance at Site 3 over water years 2019–2021. Solid trendlines show best fits for all data at high flows (percent exceedance < 30%) and at low flows (percent exceedance > 70%). Dotted trendlines show the same relationships excluding sites 1, 2 and the Western subbasin (which show consistently higher runoff).

(percent exceedance < 30%), there is a weak, but significant fit ($R^2 = 0.19$, p < 0.05). At low flows (percent exceedance > 70%) the fit improves slightly ($R^2 = 0.21$, p < 0.05). Three sites showed consistently higher runoff, falling along a trendline offset from other subbasins: 'West', 1, and 2 (Fig. 1). If we exclude these three sites from the regression analysis, we find a weak but significant fit at high flows ($R^2 = 0.07$, p < 0.05), and a strong and significant fit at low flows ($R^2 = 0.61$, p < 0.05) (Table S9).

3.2. Seasonally dynamic water storage in bofedales and their contributions to runoff

3.2.1. Bofedal material properties & water storage

Borehole transects in bofedales I-IV showed similar stratigraphy (Figs. S11 - S14): 1) hydrophytic vegetation; 2) a layer of highly

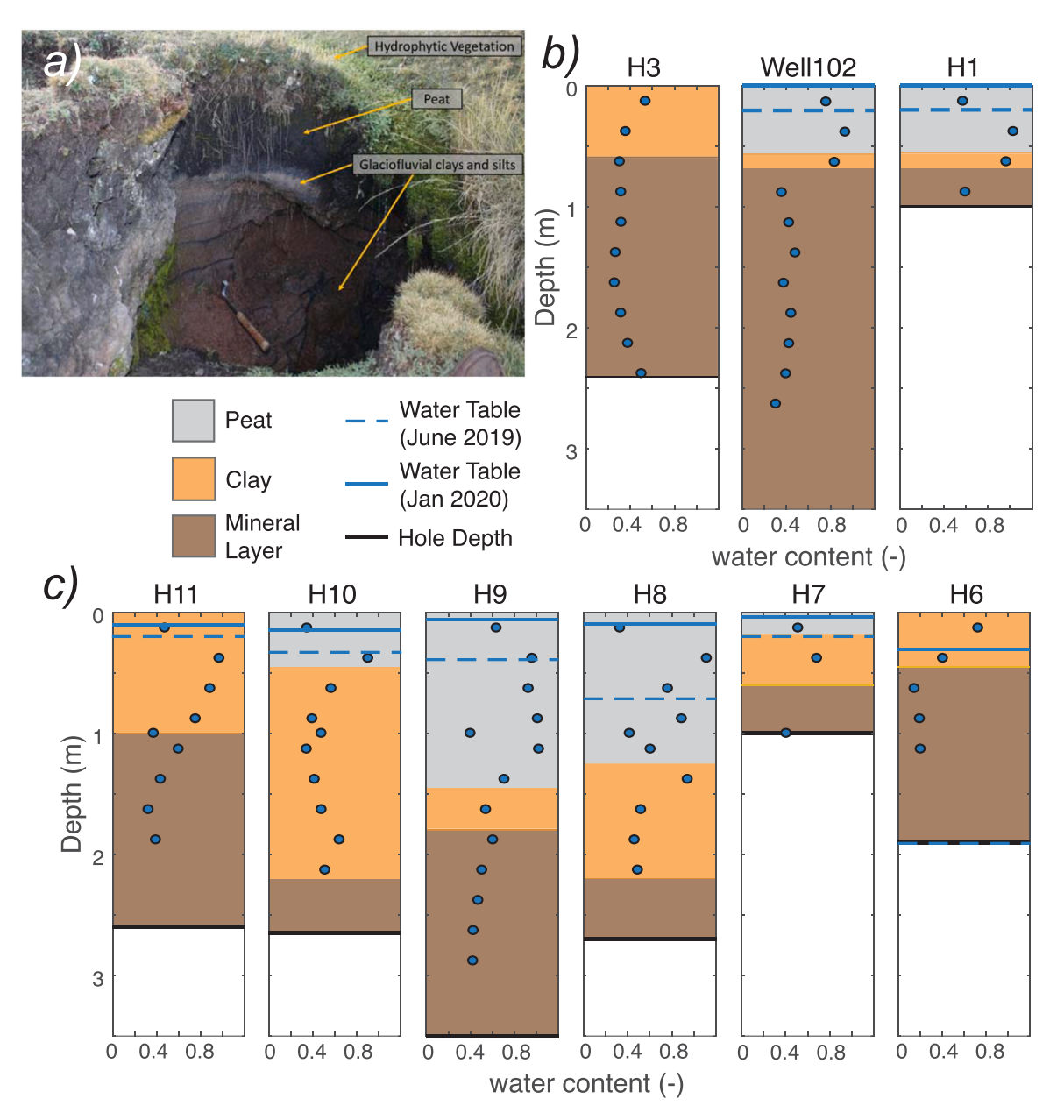


Fig. 6. a) Bofedal stratigraphy showing characteristic strata of: hydrophytic vegetation, peat, clays, and glaciofluvial deposits. Not shown is the underlying layer of weathered bedrock. Photo taken in bofedal II with a rock hammer for scale. At the time of this picture (mid dry season), water was dripping out along the boundary between the peat and glaciofluvial clay and seeping out of saturated clay. Although root density was greatest in the peat, we observed roots throughout the exposed profile. b) and c) show the results of 9 Nuclear Magnetic Resonance profiles conducted in July 2019 in bofedales I and II, respectively. The locations of boreholes are shown in Fig. S7. Profiles show peat thickening towards the center of each bofedal and pinching out at the margins. Blue dots correspond to volumetric water content (scale is at the base of each profile).

Table 5Material and hydraulic properties of the peat, clay, and mineral layers of the bofedales. Overall mean values and standard deviations were derived from 10 downhole NMR surveys conducted in June 2019. VWC and porosity reported in units of cm³/cm³. Drainable porosity is equal to the difference between mean porosity and estimated field capacity.

Subsurface stratum	Peat (0.1–1.75 m thick)	Clay (0–1.2 m thick)	Underlying mineral layer (meters thick)
Bofedal I mean porosity	0.92 ± 0.12	0.46 ± 0.13	0.38 ± 0.046
Bofedal II mean porosity	0.86 ± 0.12	0.52 ± 0.13	0.39 ± 0.046
Overall mean porosity	0.88 ± 0.12	0.51 ± 0.13	0.39 ± 0.046
Estimated VWC at field capacity	0.46	0.30	0.20
Drainable porosity	0.42	0.21	0.19
Mean saturated hydraulic conductivity (m/d)	14.3 ± 13.1	$\textbf{2.6} \pm \textbf{6.2}$	0.5 ± 0.8

Table 6 Area, upslope contributing area, and average dynamic storage in bofedales (I-IV). Final row estimates average dynamic storage applied to the $0.244 \, \mathrm{km}^2$ of bofedales scaled to represent runoff in the URW.

Site	Area (km²)	Upslope contributing area (km²)	Drainable dynamic storage (mm)
Bofedal I	0.002	0.022	390 ± 30
Bofedal II	0.085	0.428	540 ± 60
Bofedal III	0.007	0.036	430 ± 40
Bofedal IV	0.027	0.113	360 ± 30
Mean	0.030	0.150	430 ± 40

porous dark peat, greasy in texture with partially to completely decomposed organic matter up to 1.75 m thick (Table S7); 3) highly plastic glaciofluvial clays and silts up to 1.2 m thick; and 4) weathered clayey-silty saprolite or glacio-fluvial deposits that are several meters thick (photograph in Fig. 6a shows only the upper three layers). We did not observe confining layers, a perched water table, or groundwater under artesian pressure. Hydrophytic plant roots extended beyond the depth of peat into underlying clays or mineral layers (to depths exceeding 1.5 m).

Downhole NMR data from 10 borehole transects in bofedales I and II showed similar trends in the stratigraphy of different layers (with peat thickening towards the center of the bofedal) and a decrease in VWC through the profile (Fig. 6b, c). The signal to noise ratio was large, indicating the data were of high quality (Fig. S10). The porosity of each layer (determined from measurements below the June 2019 water table) showed small standard deviations across all measurements (Table 5). Drainable porosity and saturated hydraulic conductivity decreased by approximately one order of magnitude from peat to clay and from clay to the mineral layer.

3.2.2. Seasonally dynamic water storage and runoff in the URW

Average dynamic storage in bofedales I-IV varied from 360 to 540 mm (Table 6). The range is primarily due to differences in the thickness of the high porosity peat which thickened towards the center (Fig. 6b, c) and was thickest in bofedal II (1.75 m, Table S7). Smaller bofedales such as I, III, and IV, exhibited thinner peat layers (0.50 - 1.0 m).

Bofedales cover an area of $0.244~\text{km}^2$ across the URW. By combining our surveys of four bofedales with borehole NMR measurements and groundwater monitoring, we estimate bofedales store $105,000\pm10,000~\text{m}^3$ of water seasonally. At the scale of the URW $(2.12~\text{km}^2)$, this volume corresponds to $49\pm5~\text{mm}$ of water which contributes to dry season runoff once the bofedales begin to drain. Conservatively, we can compare bofedal dynamic storage to *total* dry season runoff, which averaged $73.2\pm18.2~\text{mm}$ at Site 3 and $114.9\pm21.4~\text{mm}$ at Site 1. Bofedal water storage accounts for $67\pm31\%$ of dry season streamflow at Site 3, and $43\pm22\%$ of dry season streamflow at Site 1.

4. Discussion

Andean communities depend on water resources emanating from the humid puna; however, data relating the physical structure of the humid puna, including bofedales, to hydrologic processes are limited. Here, we discuss our key findings in the context of our motivating questions by first comparing seasonal patterns in water yield from the URW with the few existing studies of water resources in high elevation and seasonally dry Andean landscapes. We next highlight our discovery of higher runoff from subbasins with greater bofedal coverage and compare seasonally dynamic storage in bofedales with dry season runoff and downstream water needs. We discuss the limitations of our analyses and present a conceptual model of the hydrologic function of bofedales in regulating water resources and sustaining perennial streamflow in the humid puna.

4.1. Water resources in the humid puna

A comparison of catchments in high elevation and seasonally dry Andean landscapes is useful to place the URW in the context of the region and to highlight similarities and differences between humid puna and more extensively studied humid páramo catchments. We compare published hydrologic and topographic data from five similar high elevation grassland catchments (Table S10). Two of the

catchments are in the seasonally dry puna of Perú and Bolivia (HUA1 and TIQ2, from Ochoa-Tocachi et al., 2016), and three are in the perennially humid páramo of southern Ecuador (PAU1 from Ochoa-Tocachi et al., 2016, and ZEO M4 and M5 from Mosquera et al., 2015).

The URW (elevation range 4011 – 4543 m.a.s.l.) lies within the elevation range of the comparison catchments, (3665 – 4840 m.a.s. l.). Nearly 16% of subbasin 3 is covered in bofedales, which is within the reported range of the 5 catchments (5 – 18%). No bofedal coverage estimates were given for PAU1 in Ochoa-Tocachi et al. (2016), so an estimate of 8% was derived using Google Earth Pro. While Ochoa-Tocachi et al. (2016) report the bofedal coverage of HUA1 to be 15%, we estimated the bofedal coverage at HUA1 to be closer to 5% using Google Earth Pro. The underlying geology of ZEO and PAU1 is predominantly composed of lava flows and ash deposits with very low permeability (Mosquera et al., 2015; Buytaert et al., 2007). The parent material weathers to form Andosols with high water retention capacity (e.g., Buytaert et al., 2006b; Buytaert and Beven, 2011; Mosquera et al., 2020b). HUA1 is a mix of sandstones and mudstones (Cobbing and Sanchez, 1996), with soils classified as Andosols and Inceptisols. Limited geological information was available for TIO2 beyond soil classification (Lepitsols and Inceptisol).

As with the URW and the larger VUB, runoff in the five catchments is driven by precipitation inputs. The URW has a slightly lower annual precipitation (803 mm) compared to the other catchments, which range from 871 mm (TIQ2) to 1358 mm (PAU1). The runoff ratio in the URW (0.57 - 0.74) was similar to runoff ratios in all catchments except for TIQ2 (0.29).

A comparison of the flow duration curves (FDC) to the two puna catchments shows the URW to have a more gentle overall slope (Fig. 7). Runoff in TIQ2 exceeds runoff in the URW during high flows and is much smaller at low flows. TIQ2's low runoff ratio and lower baseflow may be attributable to less bofedal coverage, lower average slope, large interannual storage in cirque lakes, and/or higher rates of evapotranspiration. Peak flows in HUA1 are higher than the URW, however, the slope of the FDC is large, and runoff is less than in the URW at medium to low flows (> 40% exceedance). The large slope indicates little baseflow and the flashiness of HUA1 may be a result of limited upland storage due to steep headwalls of exposed bedrock.

Runoff in the three humid páramo catchments is consistently higher than in the URW. Peak runoff is 22–78 mm/d in the humid páramo, while peak runoff in the URW reaches only 11 mm/d. In the humid páramo, large annual rainfall and no distinct dry season (Balslev and Luteyn, 1992; Luteyn, 1999; Padrón et al., 2015) results in consistent near saturation conditions in organic rich and peat-forming Histosols (wetlands) (e.g., Mosquera et al., 2015), smaller seasonal dynamics in catchment-wide water storage (e.g., Buytaert et al., 2007, Lazo et al., 2019), flashiness in peak flows (e.g. Mosquera et al., 2015; Lazo et al., 2019), and an FDC with a gentle slope. The gentle slope results from near constant rainfall, the buffering capacity of organic-rich upland Andosols (e.g., (Harden, 2006; Minaya et al., 2016; Buytaert et al., 2005), rapid development of a perched water table (e.g., Mosquera et al., 2020a), which leads to sustained recharge of wetlands and runoff generation in streams (e.g., Lazo et al., 2019; Mosquera et al., 2015, 2022).

Unlike the humid páramo, the URW experiences a dry season of approximately 5 months, and contains no Andosols, nor a perched water table in upland soils or at the soil-bedrock interface. The slope of the URW's FDC over the middle third (flow exceedance probability between 33% and 66%) is -1.49, similar to the FDC slopes of the humid páramo catchments (Table S10). In a seasonally dry environment, a gentle sloped FDC suggests the presence of dynamic water storage at the watershed scale (e.g., Searcy, 1959; Buytaert et al., 2007; Yadav et al., 2007; Ochoa-Tocachi et al., 2016). Such storage may explain recent modeling results which show high baseflow emanating from the humid puna landscape within the VUB (Fernandez-Palomino et al., 2021).

4.2. Bofedales and water yield in the URW

We found higher runoff in subbasins with greater bofedal extent. Recent studies in the humid páramo of Ecuador report similar relationships between peak runoff and wetland coverage (Mosquera et al., 2015) or between catchment wide storage and the extent of histosols (Lazo et al., 2019). The presence of wetlands in humid environments may limit catchment-wide storage capacity (e.g., Rodhe, 1989), resulting in high peak flows (Pearce, 1990; Burt, 1995; Quinton et al., 2003; Bullock and Acreman, 2003) dominated by 'event-water' (e.g., Laudon et al., 2007). The spatiotemporal patterns of runoff in the URW differ from these studies in two primary ways. First, we found no relationships between bofedal coverage or mean runoff and the size of the subbasin. Second, we found a stronger relationship between bofedal coverage and runoff at low flows, similar to studies relating greater baseflow to thicker sedimentary deposits and more extensive wetlands in boreal catchments (e.g., Karlsen et al., 2016; Floriancic et al., 2019).

Wet and dry season runoff were anomalously high at three sites in the lower part of the URW: Site 1, Site 2, and the Western subbasin. Mean slope throughout these three subbasins was between 23° and 25°, slightly steeper than in other subbasins (Table S1). Bofedales covered 11.5% and 14.5% of sites 1 and 3, respectively, but only 7.7% of the Western subbasin. Between Site 3 and Site 2, the valley morphology changes from broad and U-shaped to narrow and V-shaped with a steep, bedrock-confined channel. Changes in morphology from glaciated valleys with thick deposits to deeply incised stream morphology would decrease subsurface storage capacity as glacial deposits are removed to expose bedrock and might force flow to the surface resulting in greater stream runoff (Prancevic and Kirchner, 2019; Gillespie and Clark, 2011; Whiting and Godsey, 2016). Large runoff in the Western subbasin may be associated with extensive limestone karst in the headwaters, which are often productive water sources (e.g., Villacorta et al., 2016; Somers and McKenzie, 2020). Although there is a statistically significant fit for all data, the dry season fit improved markedly by excluding data from the three outlier catchments. The outlier catchments serve as a reminder of the additional factors (lithology and topography) controlling the hydrologic response of small (< 10 km²) upland catchments (e.g., Ochoa-Tocachi et al., 2016; Lahuatte et al., 2022) such as the URW (2.12 km²).

4.3. Dynamic storage in bofedales, quantifying contributions to streamflow

Bofedal I saturated after an average of 197 mm of cumulative precipitation, far less than the precipitation required to directly recharge one meter of peat with a porosity of 0.88 (> 880 mm). The topographic setting, temporal correspondence between hillslope field capacity and saturation in bofedal I, and a dynamic storage capacity exceeding cumulative precipitation at the time of saturation support previous studies identifying groundwater flow as the primary recharge mechanism (e.g., Cooper et al., 2019; Valois et al., 2020; Valois et al., 2021). Integrating measurements of drainable porosity in all layers over the dynamic range of the water table yields an average dynamic storage capacity of 430 mm (Table 6).

We are aware of only two studies quantifying water storage capacity in bofedales, both conducted in streamside bofedales in a narrow canyon of the Estero Derecho watershed in Chile (Valois et al., 2020; Valois et al., 2021). The Chilean bofedales are \sim 0.02 km² (smaller than bofedal IV) and composed of a \sim 0.3 m thick layer of peat and underlying fluvial deposits. The authors calculated total porosity (0.34) over a depth of 10 m to estimate a total water storage of up to 3400 mm. We suggest, however, that a more useful calculation would yield the amount of water a bofedal yields to streams. If we assume the Chilean bofedal has the same maximum water table depth as in the URW's bofedales (1.94 m), and the drainable porosities for the 0.3 m of peat and 1.64 m of underlying deposits reported in the Chilean bofedal are the same as in the URW (0.42 and 0.21, respectively), the bofedal would yield a total of 438 mm of water to streams. This brief analysis yields a comparable dynamic storage to the URW and suggests bofedales across the Andes may be contributing large volumes of water to dry season streamflow.

From the time bofedales begin to drain in the middle of the dry season (early July) to the start of the wet season (early to mid-October), irrigation demand in Zurite is approximately 730 mm (Wunderlich, 2021; Oshun et al., 2021). Chacras, or family-owned agricultural plots, are typically 0.25-1 ha $(0.0025-0.01~\text{km}^2)$ (Oshun et al., 2021). The total dynamic storage of the URW's bofedales $(105,000~\text{m}^3)$ meets the dry season irrigation demand of 13.0-15.7 ha $(0.13-0.157~\text{km}^2)$, equivalent to the needs of 13-63 chacras. Bofedales, which are fragile and vulnerable ecosystems (e.g., Bridgham et al., 2008; and Anderson et al., 2021), provide important contributions to local water supply and overall water security.

4.4. Limitations and potential error in water balance and bofedal dynamic storage estimates

4.4.1. Limitations and potential error in water balance

Our estimates of ET_a relied on the conversion of ET_a to ET_a via a crop coefficient (0.85) throughout the year in bofedales. For the uplands covered in *J. ichu*, we used a conditional model, which applies a crop coefficient (0.74) to convert ET_a to ET_a when conditions exceeded field capacity at 0.2 m depth and via direct measurements of moisture loss at conditions below field capacity. Each crop

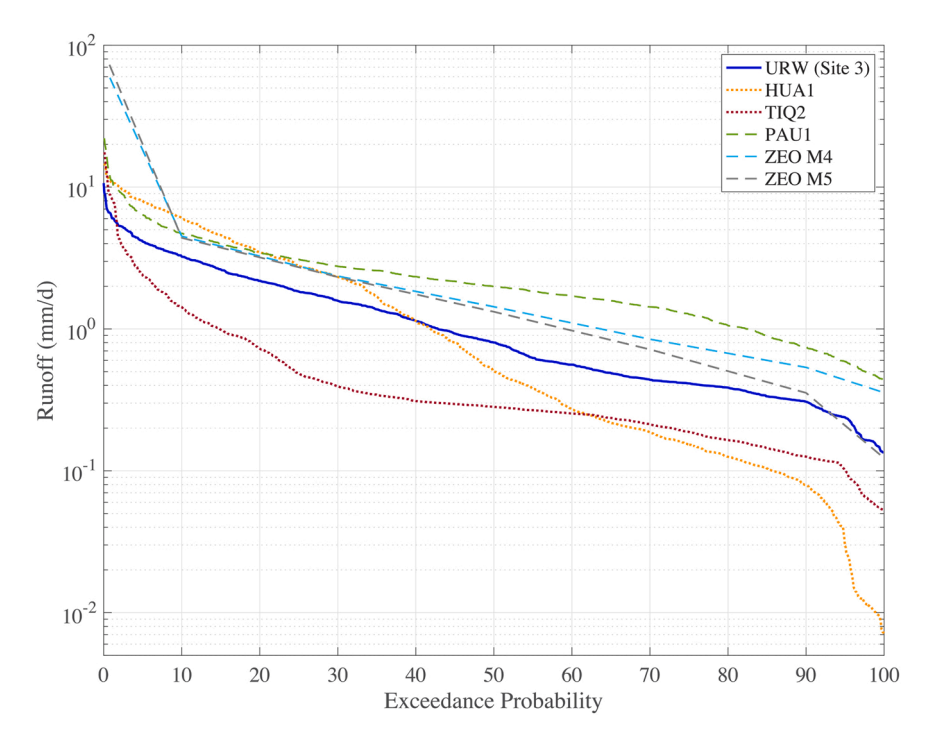


Fig. 7. Comparison of the Upper Ramuschaka Watershed flow duration curve (FDC) and published FDCs from 2 humid puna catchments (HUA1 and TIQ2 from Ochoa-Tocachi et al., 2016) and 3 páramo catchments (PAU1 from Ochoa-Tocachi et al., 2016, and ZEO M4 and M5 from Mosquera et al., 2015). For ZEO M4 and M5, published data include 0.5%, 10%, 30%, 50%, 70%, 90%, and 99.5% exceedance, only. The lack of continuous data results in straight lines in the FDCs at high and low flows.

coefficient is an imperfect fit as there are no published crop coefficients for the humid puna uplands, nor for bofedales. With each method, we report ET_a estimates and an error of 30%. Annual ET_a accounts for 34 – 35% of annual precipitation (Table 4), which corresponds well with estimates of pastureland ET_a across the VUB (Fernandez-Palomino et al., 2021), and to values reported in natural (and wetter) catchments in the páramo (Buytaert et al., 2007). However, more recent studies in the páramo report ET_a accounting for a much greater proportion of annual precipitation (e.g., Carrillo-Rojas et al., 2019; Ochoa-Sánchez et al., 2019). In WY20, greater subsurface drying (likely from vigorous vegetation growth following a grassland fire in late July 2019) resulted in a storage deficit of 69 mm (Table 4). In WY21, cumulative precipitation was larger at the time of field capacity, bofedal I saturation, and a rise in stream runoff above 1 mm/d, as greater amounts of precipitation replaced the moisture deficit across the rooting zone (Table 3). Interannual storage was 51 mm in WY21, likely due to replenishing the deficit across the rooting zone (Table 4). Whereas ET_a estimates are provided with a large range of uncertainty, the well constrained rating curves and low runoff error (12 – 13%) provide a robust estimate of water yield and corroborate the ET_a estimates.

4.4.2. Limitations and potential error in bofedal dynamic storage estimates

There are two possible sources of error in the bofedal dynamic storage estimates: spatial heterogeneity in bofedal soil properties and continuous water table dynamics across the entire URW. We have attempted to limit the extent of this error by collecting data across transects that span four bofedales covering a combined area of 0.12 km^2 (50% of the URW's total bofedal area). The transects show consistent patterns such as peat thickening towards the center of the bofedal (Fig. 6, Fig. S11-14). Furthermore, the porosity values are well constrained across the borehole transects, suggesting similar material properties across all bofedales, and the drainable porosity of peat (0.42, 47% of total porosity) is within the range of peat water yield (10 – 80%) depending on the degree of organic decomposition (Radforth and Brawner, 1977; Letts et al., 2000). We note that this is the first study to use NMR to quantify peatland water storage and highlights the value of this portable system in examining the porosity and water content within the humid puna (Fig. 6).

Despite extreme topography and a lack of road-access that required us to carry a drill rig to bofedal I, we were able to drill Well 102. However, this terrain prevented us from drilling a well in bofedal II limiting our water table measurements to one bofedal. Well 102 allowed us to measure seasonal water table fluctuations and a maximum water table depth of 1.94 m. While 1.94 m is greater than reported maximum water table depths in other bofedales (Hribljan et al., 2015; Cooper et al., 2019; Oyague et al., 2022; Monge-Salazar et al., 2022), it is similar to studies of bofedales experiencing moderate drainage (Planas-Clarke et al., 2020). In the URW, dry season drainage is likely driven by natural stream incision, which may affect the health of cushion plants despite their long taproots observed to extend to depths approaching 2 m (e.g., Chimner et al., 2019; Suarez et al., 2021; Fritz et al., 2011).

Although we do not have measurements of the maximum water table depth across all bofedales in the late dry season, our assumption of spatial consistency in groundwater dynamics is supported with the following observations: (1) The saturation of Well 102 closely followed the timing of field capacity in the hillslope, and roughly coincided with a transition to sustained high runoff values throughout the URW; and (2) similar average depths to the water table in the wet and dry seasons were found across the bofedales (Table S7). These observations would be strengthened through an expanded groundwater monitoring network, including wells in upland areas, and through the application of a conservative tracer to identify flow paths. Finally, while our site may provide insight into other similar puna grasslands catchments in the region, additional analysis at the URW and comparable analysis at other sites, including detailed information on watershed size, elevation, aspect, and geologic and hydrogeologic parameters of subsurface substrates, are needed to quantify relationships between bofedal size and dynamic water storage at the regional scale.

4.5. Conceptual model of bofedal hydrology

Bofedales contribute to catchment wide water storage and sustain baseflow through three mechanisms (Fig. 8). First, bofedales form in low gradient, glacially carved landscapes. Upland bofedales form in cirques, in which lakes or ponds become peat-forming through a process of terrestrialization. Bofedales are thus located in interior basins that, in the URW, are 4-12 times greater than the bofedal itself. Thus, bofedales intercept large volumes of groundwater, which leads to seasonal saturation. Second, layers of high porosity peat (with high drainable porosity) form a natural sponge to seasonally store tremendous volumes of water. Third, the combined effects of a low water table gradient and low hydraulic conductivities in underlying clay and mineral layers, result in the slow release of water from bofedales to streams. Although our study is the first to quantify the hydrology of bofedales in the context of water resources in the humid puna, previous studies have shown water flowing through wetlands to have longer mean transit times (e. g., Lyon et al., 2010; Roa-García and Weiler, 2010; Buytaert et al., 2011; Lane et al., 2020; Lazo et al., 2019) and argued the presence of wetlands increases or dominates the existing catchment wide water storage (e.g., Lane et al., 2020).

The impact of bofedal groundwater dynamics on streamflow is best illustrated through the three phases: 'fill-up,' 'steady-state,' and 'release.' In the fill-up phase, precipitation recharges the unsaturated zone to field capacity as the water table in bofedales continues to fall to nearly 2 m below the ground surface. After an average of 138 mm of precipitation, field capacity is reached in the upland rooting zone, causing drainage, and groundwater inflow to the bofedales. Bofedales saturate at the beginning of the steady-state phase. At this point, seasonally dynamic water storage in the URW has approached the storage capacity, and runoff rapidly increases as the catchment sheds additional precipitation. We note the likelihood of saturation overland flow across bofedales during the steady-state phase. The end of the rainy season in May – June marks the start of the release phase. Groundwater from hillslopes continues to move through bofedales to streams at rates sufficient to maintain saturation in the bofedales until an average of 41 days into the dry season, at which point the water table begins to fall at an average rate of 14 mm/day. Additional moisture depletion in the peat and clay below field capacity occurs due to transpiration of deeply rooted hydrophytic plants.

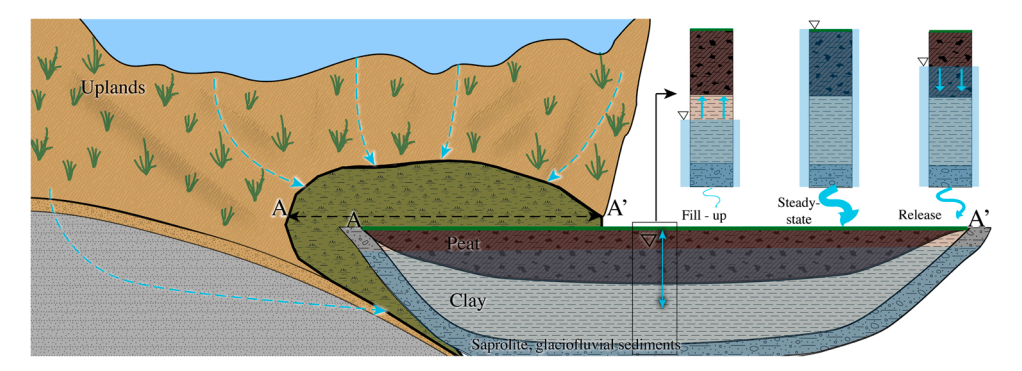


Fig. 8. We conceptualize the hydrologic function of bofedales (figure not meant to be drawn to scale) as 'way stations' at the interface between deep groundwater dynamics within the upland hillslopes and streamflow. A large contributing upland area (4–12 times the size of the bofedal) supplies groundwater to the bofedal. The bofedal is composed of layers of peat, clay and saprolite/glaciofluvial sediments. In the fill-up period, rain recharges groundwater and drives flow to bofedales, filling layers of clay and high porosity peat. Runoff in streams is small. Once the bofedal saturates, catchment wide storage capacity is filled, and successive storms generate a steady-state response generating large streamflow. In the release phase, the absence of precipitation leads to decreased groundwater contributions to bofedales and they drain slowly through low conductivity basal layers, sustaining dry season baseflow.

5. Conclusion

The URW, a $2.12~{\rm km}^2$ humid puna catchment draining to the agrarian village of Zurite, yields 57-74% of annual rainfall to runoff. Despite a dry season lasting up to 5 months, the FDC of the URW shows a gentle slope, and 12% of annual runoff comes in the dry season. The gentle slope of the FDC and sustained dry season streamflow are the result of large seasonally dynamic water storage at the catchment scale. Spatiotemporal discharge measurements throughout the URW identified greater runoff emanating from subbasins with greater bofedal coverage across all seasons. Three key characteristics provide large seasonally dynamic water storage and make bofedales vital sources of baseflow. First, bofedales are found in topographic depressions that collect water from upslope areas 4-12 times their size. Second, high porosity peat up to $1.75~{\rm m}$ thick seasonally stores tremendous volumes of water. Third, a gentle water table gradient in gently sloping bofedales and the low conductivity of underlying clay and mineral layers result in the slow drainage of stored water to streams. We estimate bofedal dynamic storage capacity and water yield to streams to be $49~{\pm}~5~{\rm mm}$ at the scale of the URW. Bofedales, which drain in the dry season, account for 20~-98% of dry season flow in the URW, sufficient to meet the irrigation demands of $13-15~{\rm ha}$. We conclude that bofedales regulate flow to sustain perennial streams in the humid puna and are thus vital to local and regional water security.

CRediT authorship contribution statement

Wyeth Wunderlich: Methodology, Formal analysis, Investigation, Data curation, Writing – original draft. Margaret Lang: Methodology, Investigation, Resources, Writing – review & editing, Supervision, Funding acquisition. Kristina Keating: Methodology, Investigation, Formal analysis, Writing – review & editing, Supervision, Funding acquisition. Wilner Bandera Perez: Investigation. Jasper Oshun: Conceptualization, Investigation, Methodology, Resources, Writing – original draft, Writing – review & editing, Supervision, Project administration, Funding acquisition.

Declaration of Competing Interest

The authors declare that they have no known competing financial interests or personal relationships that could have appeared to influence the work reported in this paper.

Data Availability

Data are available on Hydroshare, Oshun, 2023: https://www.hydroshare.org/resource/ce264199c9d1499aaa236eeaaa97b13f/.

Acknowledgements

This work would not have been possible without the support of the community of Zurite. We thank Tomás Ruiz López for his leadership in the community of Zurite and Sr. Ruiz López, Gladis Quispe, Giorgina Calanchi, Marilin Ruiz Quispe, Johannes Ruiz Quispe, and Joel Ruiz Quispe for their hospitality. Uriel Ccopa Villena provided logistical support. René Pumayalli Saloma provided rotary drilling and connected us with local geology students. Many students contributed to this research. Laurel Smith designed and executed the drone flights in 2019. Alyssa Virgil and Hannah Gidanian surveyed in most of the geospatial data. Emily Santos augered

upland boreholes and conducted grain size analyses. Nolan Marshall augered many of the bofedal boreholes, logged material layers and analyzed data. Nicholas Hawthorne selected sites and installed the stream gauges at Sites 1 and 3. Wilner Bandera was assisted in the field by Vidal Barrientos. Olivia Helprin, Jared Walbert, Edward Davis, Nolan Marshall, and Sam Bold assisted in creating the geologic map. Anna Cottrell analyzed gravimetric water content and percent carbon of bofedal peat. Other students who contributed to this work include: Peter Duin, Jillian Freiheit, Malia Gonzalez, Yojana Miraya, Hunter Murray, Johannes Ruiz Quispe, Joel Ruiz Quispe, and Logan Schmidt. Thank you to Daniel Anaya for saving our subsurface moisture equipment from a grassland fire. Thank you to Bob and Susan McPherson for donating the RTK GPS and drone. Wyeth Wunderlich was supported by the Bud Burke Scholarship and by Lost Coast Rotaract in Eureka, CA. Two anonymous reviewers provided comments that substantially improved the manuscript. This material is based on work supported by Geoscientists Without Borders (GWB), of the Society for Exploration Geophysicists under grant 2017080009 and the National Science Foundation under grants OISE-2107395 and OISE-2106297, with supplementary funding provided by a Rutgers Global Environmental Change Grant. None of the funding agencies were involved in the collection, analysis and interpretation of data, writing the manuscript, or the decision to submit the article for publication.

Appendix A. Supporting information

Supplementary data associated with this article can be found in the online version at doi:10.1016/j.ejrh.2023.101394.

References

Abdelnour, A., Stieglitz, M., Feifei, P., McKane, R., 2011. Catchment hydrological responses to forest harvest amount and spatial pattern. Water Resour. Res. 27, 9. https://doi.org/10.1029/2010WR010165.

Anderson, T.G., Christie, D.A., Chávez, R.O., Olea, M., Anchukaitis, K.J., 2021. Spatiotemporal peatland productivity and climate relationships across the western south American Altiplano. J. Geophys. Res.: Biogeosci. 126 (6) e2020JG005994.

Argüello, M., 2018. Generating critical knowledge and tools for sustainable management of water resources in the andes. Mt. Res. Dev. 38 (4), 401-403.

Aybar, C., Fernández, C., Huerta, A., Lavado, W., Vega, F., Felipe-Obando, O., 2020. Construction of a high-resolution gridded rainfall dataset for Perú from 1981 to the present day. Hydrol. Sci. J. 65 (5), 770–785. https://doi.org/10.1080/02626667.2019.1649411.

Balslev, H., Luteyn, J.L. (Eds.), 1992. Páramo: an Andean ecosystem under human influence. Academic Press, London.

Baraer, M., McKenzie, J.M., Mark, B.G., Bury, J., Knox, S., 2009. Characterizing contributions of glacier melt and groundwater during the dry season in a poorly gauged catchment of the Cordillera Blanca (Perú). Adv. Geosci. 22, 41–49.

Behroozmand, A.A., Keating, K., Auken, E., 2015. A review of the principles and applications of the NMR technique for near-surface characterization. Surv. Geophys. 36 (1), 27–85.

Bridgham, S.D., Pastor, J., Dewey, B., Weltzin, J.F., Updegraff, K., 2008. Rapid carbon response of peatlands to climate change. Ecology 89 (11), 3041–3048. https://doi.org/10.1890/08-0279.1.

Bruand, A., Tessier, D., 2000. Water retention properties of the clay in soils developed on clayey sediments: significance of parent material and soil history. Eur. J. Soil Sci. 51 (4), 679–688.

Bryant, F.C., Farfan, R.D., 1984. Dry season forage selection by Alpaca [Lama pacos] in Southern Peru. J. Range Manag. 37, 330-333.

Bullock, A., Acreman, M., 2003. The role of wetlands in the hydrological cycle. Hydrol. Earth Syst. Sci. 7, 358-389.

Burt, T.P., 1995. The role of wetlands in runoff generation from headwater catchments. In: Hughes, M.R., Heathwaite, A.L. (Eds.), Hydrology and Hydrogeochemistry of British Wetlands. Wiley, Chichester, U.K.

Buytaert, W., Beven, K., 2011. Models as multiple working hypotheses: hydrological simulation of tropical alpine wetlands (2011). Hydrol. Process. 24, 1784–1799. https://doi.org/10.1002/hyp.7936.

Buytaert, W., Wyseure, G., De Bièvre, B., & Deckers, J. (2005). The effect of land-use changes on the hydrological behaviour of Histic Andosols in South Ecuador, 3997 (August), 3985–3997. https://doi.org/10.1002/hyp.5867.

Buytaert, W., Iñiguez, V., Celleri, R., Bièvre, B.D., Wyseure, G., Deckers, J., 2006a. Analysis of the water balance of small páramo catchments in south Ecuador. In *Environmental role of wetlands in headwaters*. Springer, Dordrecht, pp. 271–281.

Buytaert, W., Célleri, R., Willems, P., De Bièvre, B., Wyseure, G., 2006b. Spatial and temporal rainfall variability in mountainous areas: a case study from the south Ecuadorian Andes. J. Hydrol. 329 (3–4), 413–421. https://doi.org/10.1016/j.jhydrol.2006.02.031.

Buytaert, W., Iñiguez, V., De Bièvre, B., 2007. The effects of afforestation and cultivation on water yield in the Andean páramo. For. Ecol. Manag. 251 (1–2), 22–30. https://doi.org/10.1016/j.foreco.2007.06.035.

Buytaert, W., Célleri, R., Timbe, L., 2009. Predicting climate change impacts on water resources in the tropical Andes: effects of GCM uncertainty. Geophys. Res. Lett. 36. 7.

Buytaert, W., Moulds, S., Acosta, L., De Bievre, B., Olmos, C., Villacis, M., Verbist, K.M., 2017. Glacial melt content of water use in the tropical Andes. Environ. Res. Lett. 12 (11), 114014.

Carlotto, V., Concha, R., Cárdenas, J., Garcia, B., Villafuerte, C. (2010) Geoloía y Geodinåamica en la Quebrada Qenqo: Aluviones que Afectaron Zurite-Cusco. Informe Tecnico. INGEMMET, UNSAAC.

Carrillo-Rojas, G., Silva, B., Rollenbeck, R., Célleri, R., Bendix, J., 2019. The breathing of the Andean highlands: net ecosystem exchange and evapotranspiration over the páramo of southern Ecuador. Agric. . Meteorol. 265, 30–47. https://doi.org/10.1016/j.agrformet.2018.11.006.

Castillo, R.M., Crisman, T.L., 2019. The role of green infrastructure in water. Energy Food Secur. Lat. Am. Caribb.

Célleri, R., Willems, P., Buytaert, W., Feyen, J., 2007. Space-time rainfall variability in the Paute Basin, Ecuadorian Andes. Hydrol. Process. 21, 3316–3327. https://doi.org/10.1002/hyp.6575.

Chimner, R.A., Bourgeau-Chavez, L., Grelik, S., Hribljan, J.A., Clarke, A.M.P., Polk, M.H., Fuentealba, B., 2019. Mapping mountain peatlands and wet meadows using multi-date, multi-sensor remote sensing in the Cordillera Blanca, Peru. Wetlands 39 (5), 1057–1067.

Cobbing and Sanchez, INGEMMET, Mapa Geoeogico del Caudrángulo de Recuay (1996).

Cooper, D.J., Wolf, E., Colson, C., Vering, W., Granda, A., Meyer, M., 2010. Alpine peatlands of the Andes, Cajamarca, Peru. Arct., Antarct., Alp. Res. 42, 19–33. Cooper, D.J., Sueltenfuss, J., Oyague, E., Yager, K., Slayback, D., Caballero, E.M.C., Mark, B.G., 2019. Drivers of peatland water table dynamics in the Central Andes, Bolivia and Perú. Hydrol. Process. 33 (13), 1913–1925. https://doi.org/10.1002/hyp.13446.

Córdova M., Carrillo-Rojas G., Crespo P., Wilcox B., Célleri R. (2015). Evaluation of the Penman-Monteith (FAO 56PM) method for calculating reference evapotranspiration using limited data. Mountain Research and Development 35(3): 230–239. DOI:10.1659/MRDJOURNAL- D-14–0024.1.

Dietrich, J. (2015). Agisoft Photoscan Crash Course. Advanced Geographic Research, online blog, accessed 10/4/2018.

Dimitrov, D.D., Lafleur, P.M., 2021. Revisiting water retention curves for simple hydrological modelling of peat. Hydrol. Sci. J. 66 (2), 252-267.

Drenkhan, F., Carey, M., Huggel, C., Seidel, J., Ore, M.T., 2015. The changing water cycle: climatic and socio-economic drivers of water-related changes in the Andes of Peru.WIREs. Water 2 (2015), 715–733.

Drenkhan, F., Guardamino, L., Huggel, C., Frey, H., 2018. Current and future glacier and lake assessment in the deglaciating vilcanota-urubamba basin, Peruvian Andes. Glob. Planet. Change 169, 105–118. https://doi.org/10.1016/j.gloplacha.2018.07.005.

Earle, L.R., Warner, B.G., Aravena, R., 2003. Rapid development of an unusual peat-accumulating ecosystem in the Chilean Altiplano. Quat. Res. 59 (1), 2–11. Engel, Z., Skrzypek, G., Chuman, T., Šefrna, L., Mihaljevič, M., 2014. Climate in the Western Cordillera of the Central Andes over the last 4300 years. Quat. Sci. Rev. 99, 60–77.

EPS SEDA CUSCO S.A. Memoria Anual 2019. Wanchaq, Cusco. (In Spanish). Accessed online January 2021. https://www.sedacusco.com/transparencia/memoria/2019.pdf.

Erickson, C.L., 2000. 12. The Lake Titicaca Basin: A Precolumbian Built Landscape. In Imperfect balance. Columbia University Press, pp. 311–356.

I.N.E.I. Estimaciónes y Proyecciones de Población Total Por Sexo de Las Principales Ciudades (2012–2015). Jesus Maria, Lima, Perú. 2015. Available online: (https://www.inei.gob.pe/estadisticas/indice-tematico/poblacion-y-vivienda/) (accessed on 15 June 2021).

Fernandez-Palomino, C.A., Hattermann, F.F., Krysanova, V., Vega-Jácome, F., Bronstert, A., 2021. Towards a more consistent eco-hydrological modelling through multi-objective calibration: a case study in the Andean Vilcanota River basin. Peru. Hydrol. Sci. J. 66 (1), 59–74.

Flores, E., Tácuna, R., & Calvo, V. (2014). Marco conceptual y metodológico para estimar el estado de salud de los bofedales. Perú. Ministerio del Ambiente.

Flores-Ochoa, J., 1977. Uywamichiq Punarunakuna. Lima, Peru: Instituto de Estudios Peruanos, Pastores de Puna

Floriancic, M.G., Fischer, B.M., Molnar, P., Kirchner, J.W., Van Meerveld, I.H., 2019. Spatial variability in specific discharge and streamwater chemistry during low flows: Results from snapshot sampling campaigns in eleven Swiss catchments. Hydrol. Process. 33 (22), 2847–2866.

Fritz, C., Pancotto, V.A., Elzenga, J.T., Visser, E.J., Grootjans, A.P., Pol, A., Smolders, A.J., 2011. Zero methane emission bogs: extreme rhizosphere oxygenation by cushion plants in Patagonia. N. Phytol. 190 (2), 398–408.

García Fernández Baca, B, 2017. Evaluación geológica y geodinámica del deslizamiento activo Llamacancha. INGEMMET. Inf. Técnico No. A 6780.

Garreaud, R.D., 2009. The Andes climate and weather. Adv. Geosci. 22, 3-11.

Glas, R., Lautz, L., McKenzie, J., Moucha, R., Chavez, D., Mark, B., Lane, J.W., 2019. Hydrogeology of an alpine talus aquifer: Cordillera Blanca, Peru. Hydrogeol. J. 27 (6), 2137–2154. https://doi.org/10.1007/s10040-019-01982-5.

Gerling, L., Weber, T.K., Reineke, D., Durner, W., Martin, S., Weber, S., 2019. Eddy covariance based surface-atmosphere exchange and crop coefficient determination in a mountainous peatland. Ecohydrology 12 (1), e2047.

Gillespie, A.R., Clark, D.H., 2011. Glaciations of the sierra Nevada, California, USA. In: Developments in Quaternary Sciences, Vol. 15. Elsevier, pp. 447–462. Gordon, R.P., Lautz, L.K., McKenzie, J.M., Mark, B.G., Chávez, D., Baraer, M., 2015. Sources and pathways of stream generation in tropical proglacial valleys of the

Cordillera Blanca, Peru. J. Hydrol. 522, 628–644. Hamon, W.R., 1963. Estimating potential evapotranspiration. Transactions of the American Society of Civil Engineers 128 (1), 324–338.

Harden, C.P., 2006. Human impacts on headwater fluvial systems in the northern and central andes. Geomorphology 79, 249-263.

Hribljan, J.A., Cooper, D.J., Sueltenfuss, J., Wolf, E.C., Heckman, K.A., Lilleskov, E.A., Chimner, R.A., 2015. Carbon storage and long-term rate of accumulation in high-altitude Andean peatlands of Bolivia. Mires Peat 15 (12), 1–14.

Hudson, R., Fraser, J., 2005. The mass balance (or dry injection) method. Streamline Watershed Manag. Bull. 9 (1), 6-12.

Ito, M., Azam, S., 2009. Engineering characteristics of a glacio-lacustrine clay deposit in a semi-arid climate. Bull. Eng. Geol. Environ. 68, 551-557.

Josse, C., Cuesta, F., Navarro, G., Barrena, V., Cabrera, E., Chacón-Moreno, E., Ferreira, W., Peralvo, M., Saito, J. & Tovar, A. (2009) Ecosistemas de los Andes del Norte y Centro. Bolivia, Colombia, Ecuador, Perú y Venezuela. (Ecosystems of Northern and Central Andes. Bolivia, Colombia, Ecuador, Peru and Venezuela). Documento Técnico, Programa Regional ECOBONA-Intercooperation, CONDESAN-Proyecto Páramo Andino, Programa BioAndes, Secretaría General de la Comunidad Andina, Lima, 96 pp. (in Spanish).

Karlsen, R.H., Grabs, T., Bishop, K., Buffam, I., Laudon, H., Seibert, J., 2016. Landscape controls on spatiotemporal discharge variability in a boreal catchment. Water Resour. Res. 52 (8), 6541–6556.

Lahuatte, B., Mosquera, G.M., Páez-Bimos, S., Calispa, M., Vanacker, V., Zapata-Ríos, X., Muñoz, T., Crespo, P., 2022. Delineation of water flow paths in a tropical Andean headwater catchment with deep soils and permeable bedrock. Hydrol. Process. 36 (10), e14725 https://doi.org/10.1002/HYP.14725.

Lane, D., McCarter, C.P., Richardson, M., McConnell, C., Field, T., Yao, H., Mitchell, C.P., 2020. Wetlands and low-gradient topography are associated with longer hydrologic transit times in Precambrian Shield headwater catchments. Hydrol. Process. 34 (3), 598–614.

Lane, K., 2009. Engineered highlands: the social organization of water in the ancient north-central Andes (AD 1000–1480). World Archaeol. 41 (1), 169–190. Laudon, H., Sjoblom, V., Buffam, I., Seibert, J., Morth, M., 2007. The role of catchment scale and landscape characteristics for runoff generation of boreal streams.

J. Hydrol. 344, 198–209.
Lazo, P.X., Mosquera, G.M., McDonnell, J.J., Crespo, P., 2019. The role of vegetation, soils, and precipitation on water storage and hydrological services in Andean Páramo catchments. Journal of Hydrology 572, 805–819.

Letts, M.G., Roulet, N.T., Comer, N.T., Skarupa, M.R., Verseghy, D.L., 2000. Parametrization of peatland hydraulic properties for the Canadian Land Surface Scheme. Atmosphere-Ocean 38 (1), 141–160.

López Gonzales, M., Hergoualc'h, K., Angulo Núñez, O., Baker, T., Chimner, R., del Águila Pasquel, J., del Castillo Torres, D., Freitas Alvarado, L., Fuentealba Durand, B., García Gonzales, E., Honorio Coronado, E., Kazuyo, H., Lilleskov, E., Málaga Durán, N., Maldonado Fonkén, M., Martín Brañas, M., Vargas, T.M., Planas Clarke, A.M., Roucoux, K., Vacalla Ochoa, F., 2020. What do we know about Peruvian peatlands? In: CIFOR Occasional Paper no. 210 Bogor, Indonesia. https://doi.org/10.17528/cifor/007848.

Luteyn, J.L., 1999. Páramos: A Checklist of Plant Diversity, Geographical Distribution, and Botanical Literature. Botanical Garden Press, Bronx.

Lyon, S.W., Laudon, H., Seibert, J., Mörth, M., Tetzlaff, D., Bishop, K.H., 2010. Controls on snowmelt water mean transit times in northern boreal catchments. Hydrol. Process. 24 (12), 1672–1684.

Maldanado Fónken, M., 2014. An introduction to the bofedales of the Peruvian High Andes. Mires Peat 15 (4), 1-13.

Minaya, V., Corzo, G., van der Kwast, J., Mynett, A.E., 2016. Simulating gross primary production and stand hydrological processes of páramo grasslands in the ecuadorian andean region using the Biome-BGC model. Soil Sci 181, 335–346. https://doi.org/10.1097/SS.0000000000000154.

Ministry of the Environment, 2019. Guía de evaluación del estado del Ecosistema de bofedal. Minist. Environ.

Monge-Salazar, M.J., Tovar, C., Cuadros-Adriazola, J., Baiker, J.R., Montesinos-Tubée, D.B., Bonnesoeur, V., Buytaert, W., 2022. Ecohydrology and ecosystem services of a natural and an artificial bofedal wetland in the central Andes. Sci. Total Environ. 838, 155968.

Mosquera, G., Lazo, P., Celleri, r, Wilcox, B., Crespo, P., 2015. Runoff from tropical alpine grasslands increases with areal extent of wetlands. Catena 125, 120–128 (2015).

Mosquera, G.M., Crespo, P., Breuer, L., Feyen, J., Windhorst, D., 2020. Water transport and tracer mixing in volcanic ash soils at a tropical hillslope: a wet layered sloping sponge. Hydrol. Process. 34 (9), 2032–2047.

Mosquera, G.M., Marín, F., Stern, M., Bonnesoeur, V., Ochoa-Tocachi, B.F., Román-Dañobeytia, F., Crespo, P., 2022. Progress in understanding the hydrology of high-elevation Andean grasslands under changing land use. Sci. Total Environ. 804, 150112.

Municipalidad Distrital de Zurite. (2017). Plan de Desarrollo Concertado del Distrito de Zurite al 2017 (Spanish). Accessed online: (https://www.scribd.com/document/436252392/PLAN-DE-DESARROLLO-CONCERTADO-DEL-DISTRITO-DE-ZURITE-AL-2017).

Ochoa-Sánchez, A., Crespo, P., Carrillo-Rojas, G., Sucozhañay, A., Célleri, R., 2019. Actual evapotranspiration in the high andean grasslands: a comparison of measurement and estimation methods. Front. Earth Sci. 7, 55. https://doi.org/10.3389/feart.2019.00055.

Ochoa-Tocachi, B., et al., 2016. Impacts of land use on the hydrological response of tropical Andean catchments. Hydrol. Process. https://doi.org/10.1002/hyp.10980.

Oshun, J., Keating, K., Lang, M., Miraya Oscco, Y., 2021. Interdisciplinary water development in the peruvian highlands. Case Incl. Coprod. Knowl. Socio-Hydrol. Hydrol. 8 (3), 112.

- Oshun, J., 2023. The role of peat-forming bofedales in sustaining baseflow in the humid puna. HydroShare. http://www.hydroshare.org/resource/ce264199c9d1499aaa236eeaaa97b13f.
- Oyague, E., Cooper, D.J., Ingol, E., 2022. Effects of land use on the hydrologic regime, vegetation, and hydraulic conductivity of peatlands in the central Peruvian Andes. J. Hydrol. 609, 127687.
- Padrón, R.S., Wilcox, B.P., Crespo, P., Célleri, R., 2015. Rainfall in the Andean Páramo: new insights from high-resolution monitoring in Southern Ecuador. J. Hydrometeorol. 16 (3), 985–996. https://doi.org/10.1175/JHM-D-14-0135.1.
- Palacios Rios F. 1977. Pastizales de regadío para alpacas [in Spanish]. In: Flores Ochoa J.A., editor. Pastores de puna: Uywamichiq Punarunakuna. Lima, Peru: Instituto de Estudios Peruanos, pp 155–170.
- Parra, B.G., Rojas, L.E.P., Barrios, M., Estrada, J.C.M., 2016. Uncertainty of discharge estimation in high-grade Andean streams. Flow. Meas. Instrum. 48, 42–50. Patty, L., Halloy, S.R., Hiltbrunner, E., et al., 2010. Biomass allocation in herbaceous plants under grazing impact in the high semi-arid Andes. Flora-Morphol., Distrib., Funct. Ecol. Plants 205, 695–703.
- Pearce, A.J., 1990. Streamflow generation processes—an austral view. Water Resour. Res. 26, 3037-3047.
- Planas-Clarke, A.M., Chimner, R.A., Hribljan, J.A., Lilleskov, E.A., Fuentealba, B., 2020. The effect of water table levels and short-term ditch restoration on mountain peatland carbon cycling in the Cordillera Blanca. Peru. Wetl. Ecol. Manag. 28, 51–69.
- Polk, M.H., Young, K.R., Cano, A., Leon, B., 2019. Vegetation of Andean wetlands (bofedales) in Huascarán National Park, Peru (2019), Article 01 Mires Peat Volume 24, 1–26. https://doi.org/10.19189/MaP.2018.SNPG.387.
- Prancevic, J.P., Kirchner, J.W., 2019. Topographic controls on the extension and retraction of flowing streams. Geophys. Res. Lett. 46 (4), 2084–2092.
- Quinton, W.L., Hayashi, M., Pietroniro, A., 2003. Connectivity and storage functions of channel fens and flat bogs in northern basins. Hydrol. Process. 17, 3665–3684. Radforth, N.W., & Brawner, C.O. (1977). Muskeg and the northern environment in Canada. In Muskeg Research Conference 1973: Edmonton, Alta.). University of Toronto Press.
- Reiner, R.J., Bryant, F., 1986. Botanical composition and nutri-tional quality of alpaca diets in two Andean rangeland com-munities. J. Range Manag. 39, 424–427. Roa-García, M.C., Weiler, M., 2010. Integrated response and transit time distributions of watersheds by combining hydrograph separation and long-term transit time modeling. Hydrol. Earth Syst. Sci. 14 (8), 1537–1549.
- Rodhe, A., 1989. On the generation of stream runoff in till soils: paper presented at the nordic hydrological conference (Rovaniemi, Finland, August-1988). Hydrol. Res. 20 (1), 1–8.
- Salvador, F., Monerris, J., Rochefort, L., 2014. Peatlands of the Peruvian Puna ecoregion: types, characteristics and disturbance. Mires Peat 15 (article 03), 1–17. Sayama, T., McDonnell, J.J., Dhakal, A., Sullivan, K., 2011. How much water can a watershed store? Hydrol. Process. 25, 3899–3908. https://doi.org/10.1002/hyp.8288.
- Schmidt, L., Rempe, D., 2020. Quantifying dynamic water storage in unsaturated bedrock with borehole nuclear magnetic resonance. Geophys. Res. Lett. 47 (22) e2020GL089600.
- Searcy, J.K. (1959). Flow-duration curves (No. 1542). US Government Printing Office.
- Somers, L.D., McKenzie, J.M., 2020. A review of groundwater in high mountain environments, 7. Wiley Interdisciplinary Reviews: Water, e1475.
- Somers, L.D., McKenzie, J.M., Mark, B.G., Lagos, P., Ng, G.H.C., Wickert, A.D., Silva, Y., 2019. Groundwater buffers decreasing glacier melt in an Andean watershed—but not forever. Geophys. Res. Lett. 46 (22), 13016–13026.
- Squeo, F.A., Warner, B., Aravena, R., Espinoza, D., 2006. Bofedales: high altitude peatland of the central Andes. Rev. Chil. De. Hist. Nat. 79, 245-255.
- Suarez, E., Chimbolema, S., Chimner, R.A., Lilleskov, E.A., 2021. Root biomass and production by two cushion plant species of tropical high-elevation peatlands in the Andean paramo. Mires Peat. 27 (18), 1–9.
- Tovar, C., Arnillas, C.A., Cuesta, F., Buytaert, W., 2013. Diverging responses of tropical Andean biomes under future climate conditions. PloS One 8 (5), e63634. Uribe-Álvarez, M.C., Prieto, M., Meseguer-Ruiz, O., 2022. Bofedal response to climate variability, local management, and water extraction: A case study of Chucuyo, Northern Chile. J. Mt. Sci. 19 (1), 241–252.
- USGS (2017). Unmanned Aircraft Systems Data Post-Processing. United States Geological Survey. UAS Federal Users Workshop 2017, https://uas.usgs.gov/pdf/PhotoScanProcessingDSLRMar2017.pdf, consulted at 30 of July 2018.
- Valois, R., Schaffer, N., Figueroa, R., Maldonado, A., Yáñez, E., Hevia, A., MacDonell, S., 2020. Characterizing the water storage capacity and hydrological role of mountain peatlands in the arid andes of North-Central Chile. Water 12 (4), 1071.
- Valois, R., Araya Vargas, J., MacDonell, S., Guzmán Pinones, C., Fernandoy, F., Yánez Carrizo, G., Maldonado, A., 2021. Improving the underground structural characterization and hydrological functioning of an Andean peatland using geoelectrics and water stable isotopes in semi-arid Chile. Environ. Earth Sci. 80 (1), 1–14.
- Villacorta, S., Rodríguez, C., Peña, F., Jaimes, F. y, Luza, C., 2016. Caracterización geodinámica y dendrocronología como base para la evaluación de procesos geohidrológicos en la cuenca del río Mariño, Abancay (Perú). Ser. Correl. Geol. 32 (1–2), 25–42.
- Vining, B.R., Steinman, B.A., Abbott, M.B., Woods, A., 2019. Paleoclimatic and archaeological evidence from Lake Suches for highland Andean refugia during the arid middle-Holocene. Holocene 29 (2), 328–344.
- Walsh, D., Turner, P., Grunewald, E., Zhang, H., Butler, Jr, J.J., Reboulet, E., Fitzpatrick, A., 2013. A small-diameter NMR logging tool for groundwater investigations. Groundwater 51 (6), 914–926.
- White-Nockleby, C., Prieto, M., Yager, K., Meneses, R.I., 2021. Understanding bofedales as cultural landscapes in the central Andes. Wetlands 41 (8), 1–14. Whiting, J.A., Godsey, S.E., 2016. Discontinuous headwater stream networks with stable flowheads, Salmon River basin, Idaho. Hydrol. Process. 30 (13), 2305–2316. Wunderlich, W., 2021. Spatiotemporal patterns in water yield from the humid puna: a case study in the agrarian district of Zurite. Perú.
- Yadav, M., Wagener, T., Gupta, H., 2007. Regionalization of constraints on expected watershed response behavior for improved predictions in ungauged basins. Adv. Water Resour. 30, 1756–1774. https://doi.org/10.1016/j.advwatres.2007.01.005.
- Yager, K., Prieto, M., Meneses, R.I., 2021. Reframing pastoral practices of bofedal management to increase the resilience of andean water towers. Mt. Res. Dev. 41 (4), A1–A9.